Journal of Solid State Chemistry 333 (2024) 124639

Contents lists available at ScienceDirect

Journal of Solid State Chemistry

journal homepage: www.elsevier.com/locate/jssc

Structure directing factors and photophysical properties of five Cu(I)-iodide materials with N-donor heteroaromatic ligands

Francisco Sánchez-Férez [a], Xavier Solans-Monfort [a], Luis Rodríguez-Santiago [a], Teresa Calvet [b], Mercè Font-Bardia [c], Josefina Pons [a,*]

[a] Departament de Química, Universitat Autònoma de Barcelona, 08193, Bellaterra, Barcelona, Spain
[b] Departament de Mineralogia, Petrologia i Geologia Aplicada, Universitat de Barcelona, Martí i Franquès s/n, 08028, Barcelona, Spain
[c] Unitat de Difracció de Raig-X, Centres Científics i Tecnològics de la Universitat de Barcelona (CCiTUB), Universitat de Barcelona, Solé i Sabarís, 1-3, 08028, Barcelona, Spain

ARTICLE INFO

Keywords:
Heteroaromatic ligands
Cu(I) iodide
Coordination polymers
Tetrameric cubane
Light emitting materials
TD-DFT calculations

ABSTRACT

In this work, two families of Cu(I)-iodide complexes with *N*-heterocyclic donors ligands bearing amide, phenyl, chloro, and methyl substituents have been synthesized to combine two structural directing factors: attractive interactions and steric bulkiness. To this aim, we synthesized five Cu(I)-iodide based complexes: two 1D coordination polymers $[CuI(isn)]_n$ (**1**) and $\{[CuI(nic)]\cdot ACN\}_n$ (**2**), one tetrameric cubane $[CuI(3\text{-}phpy)]_4$ (**3**), one rhomboid dimer $[CuI(8\text{-}ClQuin)]_2$ (**4**) and one monomer $[CuI(1\text{-}CH_3isoQuin)]$ (**5**). Interestingly, easy ligand dissociation and marked distortions within the molecular structure enabled structural rearrangements between the mentioned arrays. Then, we compiled the structures contained in this family of materials and provided a shape map and a conversion pathway between the most similar arrays, the cubane and the staircase polymer. Finally, the photophysical properties of **1**–**5** were investigated and electronic transitions were identified and supported by DFT and TD-DFT calculations since their photophysical properties are strongly dependent on the molecular arrangement and electronic distribution.

1. Introduction

Semiconductor based materials are being increasingly exploited for their interesting applications as catalysts [1], photocatalysts and photo-electrocatalysts [2] but, even more, for their outstanding performance in the field of solid-state lighting (SSL) as light emitting devices (LEDs) [3]. Cu(I) iodide hybrid materials are aimed to be the grounding for the next generation of LEDs benefiting from their improved and longer lasting electricity to light conversion, solution processability [4], cost-effectiveness, and easy preparation [5].

The combination of Cu(I) iodide, nurturing from a d^{10} electron configuration and deprived of non-emissive metal-centered transitions, with *N*-, *S*- or *P*-donor aromatic ligands have the uniqueness of highly tunable photophysical properties with high quantum yields, exhibiting emission throughout the entire visible spectra, as well as, UV and near-infrared (NIR) edge [6]. Their flexible coordination environment gives access to a bounded range of arrangements, rendering coordination numbers between two and four, and distorted intermediate geometries from linear to tetrahedral. This great structural variety dictates the resulting photophysical properties, establishing these materials as a prime example of structure-property relationship and highlighting the need to get a further understanding of structure-directing factors.

The most accessible architectures bearing Cu–N dative bonds from pyridine and monodentate derivatives in that order are the polymeric 1D staircase chain, the cubane tetrameric cluster $[Cu_4I_4(L)_4]$, the rhomboid dimer, and the monomer, which tends, *per se*, to accommodate four coordinated Cu(I) centers except for sterically demanding ligands able to force trigonal planar geometries [7]. Nevertheless, this set of arrangements can be accessed by a single ligand and the formation of the molecular array will be determined by both the experimental conditions *inter alia* temperature, CuI:L ratio or solvent, and the steric requirements of the ligand [8]. Hence, their structural versatility and interconversion entail that crystal engineering of Cu(I)-iodide materials is still a challenging research field. Indeed, many ligands have exhibited the capability to be arranged into several of the aforementioned arrays [9–11], including mixtures of them, and in some cases have even gotten access to less common architectures *inter alia* the octahedral tetramer [12] and the hexameric "eared" cubane [13,14].

* Corresponding author.
E-mail address: Josefina.Pons@uab.es (J. Pons).

https://doi.org/10.1016/j.jssc.2024.124639
Received 19 January 2024; Received in revised form 22 February 2024; Accepted 23 February 2024
Available online 28 February 2024

As stimuli-responsive materials, Cu(I)-iodides are an archetypal family of temperature-dependent emitters [15], referred to as thermochromic, being their emission markedly sensitive to temperature. This has been attributed to the enhancement of cluster-centered (^{3}CC) transitions as a result of shrunk Cu···Cu distances in the excited state [16]. Indeed, this property is frequently reported for Cu(I)-iodide clusters that have the particularity of exhibiting two emission bands, denoted as high energy (HE) and low energy (LE). The HE band originates from iodide to ligand charge transfer (^{3}XLCT) transitions, with the potential contribution of metal to ligand charge transfer (MLCT), whereas the LE band implies ^{3}CC transitions [17]. Variations of their emission properties, for instance, their relative intensities or shift of the emission wavelength, especially for LE bands, are strongly related to Cu–I bond lengths and cuprophilic interactions upon changes in Cu···Cu distances below 2.8 Å, which is the sum of the van der Waals radii of Cu(I). Interestingly, *N*-donor ligands usually promote shorter Cu···Cu distances, which fall below this threshold, and enhance emission from ^{3}CC states [18]. This behavior can provide access to electronic transitions involving molecular orbitals of different natures, caused by rigidification and the consequent shortening of Cu···Cu and Cu–I distances [19]. Likewise, staircase chain CuI(L) arrangements are thought to emit by M(X)LCT and can also exhibit dual luminescence arising from ^{3}CC and 1D delocalized transitions [20]. Besides, cubane and rhomboid dimer arrays have already demonstrated superior luminescence performance also based on M(X)LCT emission, through reduced nonradiative processes due to hindered cuprophilic interactions with longer Cu···Cu distances [21]. Noteworthy, DFT calculations suggested that electronic properties from the clusters are kept when using them as building blocks to achieve increased dimensionality [22].

The proper synthetic conditions for the arrangement of rhomboid dimers, staircase polymers and tetrameric cubanes are still an intriguing issue since even mixtures or interconversion between these different isomeric forms have been reported and are dependent on subtle changes in the synthetic conditions. This could indicate that the different arrangements are close in energy and the stabilization of one or another can be easily biased towards one specific array. Among them, one-pot synthesis provides a straightforward methodology for the synthesis of homoleptic Cu(I)-iodide complexes but lacks the control of nuclearity. Instead, it usually employs a combination of specific experimental conditions such as the reaction ratio, solvent, or concentration, which makes it possible to determine the final arrangement. Besides, the combination of the strong ionic character of Cu–I bond and the weaker nature of the Cu–N bond provides the perfect scenario for structural transformations in solution. To avoid these drawbacks, the incorporation of structure directing factors such as strong intermolecular interactions or steric effects could confer the required degree of control and make feasible the use of one-pot reactions for the synthesis of Cu(I)-iodide complexes.

Our group is working on the structure-property relations of different d^{10} metal complexes bearing *N*-donor heteroaromatic ligands [23,24] and, recently, a new family of *N*-substituted carboranyl pyrazole based Cu(I)-iodide emitters was reported [17]. Continuing with this research, we provide the rational synthesis of five Cu(I)-iodide based materials containing either pyridine, quinoline or isoquinoline derivatives with markedly different photophysical properties. Therefore, we have performed the reaction between CuI and 4-pyridinecarboxamide (isonicotinamide, isn) or 3-pyridinecarboxamide (nicotinamide, nic) benefiting from their strong amide···amide homosynthon to bias the resulting arrangement. Indeed, the biased assembly of amide···amide interactions in primary amides template supramolecular polymeric arrangements [25]. We also introduced 3-phenylpyridine (3-phpy) that should act as an unbiasing ligand. Then, the incorporation of 8-chloroquinole (8-ClQuin) provided bulkiness but attractive interactions to the Cu(I) center whereas the use of 1-methylisoquinoline (1-CH_3isoQuin) exacerbates steric hindrance. Reactions with isn and nic resulted in the formation of 1D double stranded coordination polymers [CuI(isn)]$_n$ (**1**) and {[CuI(nic)]·ACN}$_n$ (**2**), whereas the use of 3-phpy brough to a cubane structure [CuI(3-phpy)]$_4$ (**3**). Interestingly, the addition of 8-ClQuin or 1-CH_3isoQuin forced the arrangement of the rhomboid dimer {[CuI(8-ClQuin)]·8-ClQuin}$_2$ (**4**) or the monomer [CuI(1-CH_3isoQuin)$_2$] (**5**) (Scheme 1). Their photophysical properties were analyzed through solid state UV–Vis and fluorescence and better understood by TD-DFT calculations.

2. Experimental section

2.1. Materials and general details

Cu(I) iodide (CuI), 4-pyridinecarboxamide (isonicotinamide, isn), 3-pyridinecarboxamide (nicotinamide, nic), 3-phenylpyridine (3-phpy), 8-chloroquinoline (8-ClQuin) and 1-methylisoquinoline (1-CH_3isoQuin) ligands, potassium iodide (KI) as well as acetonitrile (ACN), diethyl ether (Et_2O) and acetone as solvents were purchased from Sigma-Aldrich. The water used was MilliQ. Deuterated acetonitrile (ACN-d_3) was used for the ^{1}H NMR experiments, and it was purchased from Eurisotop. All of them were commercially available and used without further purification.

Reactions and manipulation were carried out in air at room temperature (RT). Elemental analyses (C, H, N) were carried out on a Euro Vector 3100 instrument. FTIR-ATR spectra were recorded on a PerkinElmer spectrometer equipped with a universal attenuated total reflectance (ATR) accessory with a diamond window in the range from 4000 to 500 cm^{-1}. ^{1}H NMR spectra were recorded on an NMR Bruker Ascend 400 MHz spectrometer in ACN-d_3 solution at RT. All chemical shifts (δ) are given in ppm, referenced to the residual solvent peak and coupling constants in Hertz. Multiplets nomenclature is as follows: singlet (s); doublet (d); doublet of doublets (dd); broad (br); multiplet (m). Solid-state UV–Vis experiments were performed with a Cary 4000 UV–Vis spectrophotometer between 200 and 800 nm. Solid-state photoluminescence measurements were recorded using a Varian Cary Eclipse Fluorescence spectrophotometer between 350 and 700 nm. CIE 1931 chromaticity diagram was generated using Origin Pro 2019b software.

2.2. Synthesis of complexes *1–3*

To a 5 mL ACN solution of CuI (100 mg, 0.525 mmol), 4 mL of an ACN solution containing the dPy (isn (**1**), nic (**2**) and 3-phpy (**3**)) were added dropwise (64.1 mg, 0.525 mmol (**1**); 64.5 mg, 0.528 mmol (**2**); and 75.3 μL, 0.525 mmol (**3**). Immediately after the addition of the dPy, a white (**1**) or yellowish (**2** and **3**) powder was formed. Then, they were sonicated for 10 min. In the case of **2**, the suspension was redissolved. The solids (**1–3**) were filtered and washed twice with 10 mL of cold acetone. Then they were dried under vacuum for 1 h.

[CuI(isn)]$_n$ (**1**). Yield: 136 mg (83%). Anal. Calc. for $C_6H_6N_2OICu$ (312.57 g mol^{-1}): C, 23.06; H, 1.93; N, 8.96%. Found: C, 23.01; H, 1.87; N, 8.82%. FTIR-ATR (wavenumber, cm^{-1}): 3415 (m) [υ(N–H)]$_{as}$, 3293 (w) [υ(N–H)]$_{as}$, 3140(m) [υ(N–H)]$_s$, 3088(w) - 3039(w) [υ(C–H)]$_{ar}$, 1691(s) [υ(C═O)], 1621(m) [υ(C═C/C═N)], 1605(m) [υ(C═C/C═N)], 1547(m) [δ(N–H)], 1494(w) [υ(C–NH_2)], 1415(m) [δ(C═C/C═N)], 1379(s) [δ(C═C/C═N)], 1217(m), 1149(w), 1113(m), 1059 (m) [δ(C–H)]$_{ip}$, 1018(m) [δ(C–H)]$_{ip}$, 846(m) [δ(C–H)]$_{oop}$, 761(m) [δ(C–H)]$_{oop}$, 688(w), 644(s), 542(m). ^{1}H NMR (400 MHz; ACN-d_3; 298 K): δ = 8.70 [2H, d, ^3J = 5.9 Hz, o-*H*], 7.67 [2H, d, ^3J = 6.0 Hz, m-*H*], 6.90 [1H, s, -NH_{syn}], 6.19 [1H, s, -NH_{anti}].

{[CuI(nic)]·ACN}$_n$ (**2**). Yield: 148 mg (80%). Anal. Calc. for $C_8H_9N_3OICu$ (353.62 g mol^{-1}): C, 27.17; H, 2.57; N, 11.88%. Found: C, 27.22; H, 2.61; N 11.80%. FTIR-ATR (wavenumber, cm^{-1}): 3402 (m) [υ(N–H)]$_{as}$, 3316(w) [υ(N–H)]$_{as}$, 3172(m) [υ(N–H)]$_s$, 3063(w) [υ(C–H)]$_{ar}$, 2991(w) [υ(C–H)]$_{ar}$, 2935(w), 2781(w), 2287(w) [δ(C–H)+υ(C–C)]$_{ACN}$, 2256(w) [υ(C≡N)]$_{s,\ ACN}$, 1689(s) [υ(C═O)], 1626(m) [υ(C═C/C═N)], 1592(m) [υ(C═C/C═N)], 1572(m)

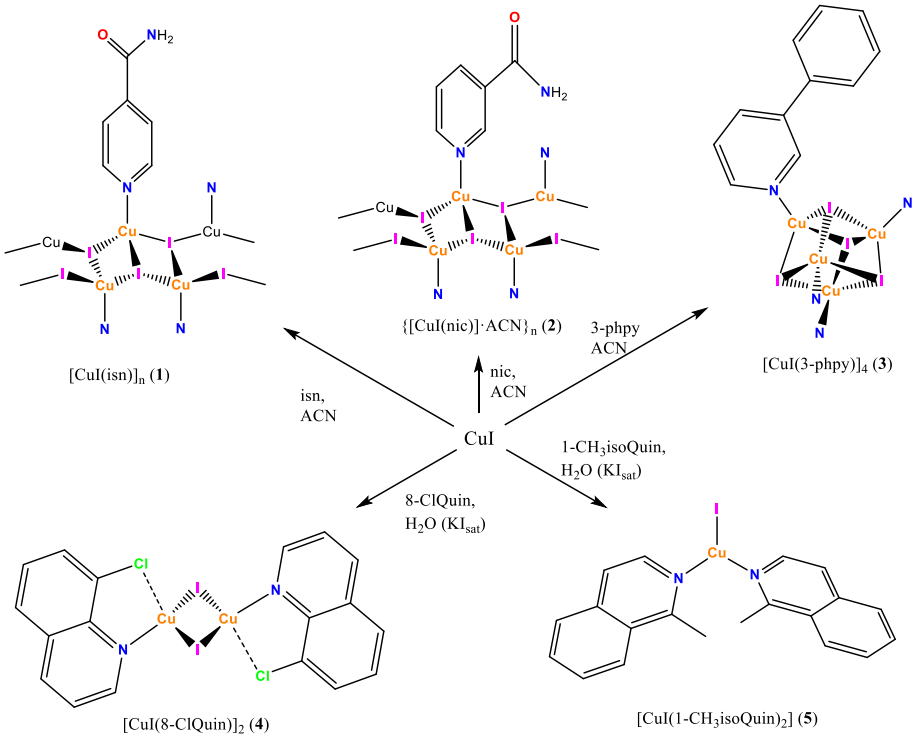

Scheme 1. Outline of the synthesis of complexes **1**–**5**.

[δ(N–H)], 1474(w) [υ(C–NH_2)], 1435(m) [δ(C═C/C═N)], 1393 (s) [δ(C═C/C═N)], 1383(s) [δ(C═C/C═N)], 1358(m) [δ(C–H_3)]$_{s,\ ACN}$, 1192(m), 1140(m), 1043(m) [δ(C–H)]$_{ip}$, 1029(m) [δ(C–H)]$_{ip}$, 991(w), 960(w), 924(w) [υ(C–C)]$_{ACN}$, 829(w), 783(br) [δ(C–H)]$_{oop}$, 722(w), 691 (s) [δ(C–H)]$_{oop}$, 654(s) [δ(C–H)]$_{oop}$, 639(m), 554(s), 511(s). ^{1}H NMR (400 MHz; ACN-d_3; 298 K): δ = 8.97 [1H, s, o-*H*-C], 8.69 [1H, d, ^3J = 4.1 Hz, o-*H*-CH], 8.12 [1H, dd, ^3J = 7.9 Hz, ^4J = 1.6 Hz, p-*H*], 7.43 [1H, dd, ^3J = 7.6 Hz, ^3J = 4.8 Hz, m-*H*], 6.83 [1H, s, -NH_{syn}], 6.10 [1H, s, -NH_{anti}].

[CuI(3-phpy)]$_4$ (**3**). Yield: 144 mg (79%). Anal. Calc. for $C_{44}H_{36}N_4I_4Cu_4$ (1382.53 g mol^{-1}): C, 38.22; H, 2.62; N, 4.05%. Found: C, 38.30; H, 2.55; N, 4.11%. FTIR-ATR (wavenumber, cm^{-1}): 3057(w) - 3023(w) [υ(C–H)]$_{ar}$, 2944(w), 1595(w) [υ(C═C/C═N)], 1579(w) [υ(C═C/C═N)], 1469(m) [υ(C═C/C═N)], 1446(m) [δ(C═C/C═N)], 1407(m) [δ(C═C/C═N)], 1391(sh), 1328(w), 1312(w), 1295(w), 1279 (w), 1242(w), 1225(w), 1191(m), 1177(w), 1152(w), 1131(w), 1104 (m), 1071(m) [δ(C–H)$_{ip}$, 1033(m) [δ(C–H)]$_{ip}$, 1013(m) [δ(C–H)]$_{ip}$, 994 (w), 944(w), 930(w), 917(w), 845(w), 813(m) [δ(C–H)]$_{oop}$, 758(s) [δ(C–H)]$_{oop}$, 699(s) [δ(C–H)]$_{oop}$, 671(m), 648(m), 624(m), 555(m), 511 (m), 501(m). ^{1}H NMR (400 MHz; ACN-d_3; 298 K): δ = 8.85 [1H, s, *o-H*$_{py}$-C], 8.56 [1H, d, ^3J = 4.7 Hz, *o-H*$_{py}$-CH], 8.00 [1H, dd, ^3J = 8.0 Hz, ^4J = 1.6 Hz, *p-H*$_{py}$], 7.66 [2H, d, ^3J = 7.1 Hz, ^4J = 1.7 Hz, *o-H*$_{ph}$], 7.50 [2H, m, *m-H*$_{ph}$], 7.43 [2H, m, *m-H*$_{py}$ + *p-H*$_{ph}$].

2.3. Synthesis of complexes *4* and *5*

For the synthesis of **4** and **5**, to a 5 mL of a KI saturated aqueous solution with CuI (100 mg, 0.525 mmol), 5 mL of an ACN solution of 8-ClQuin (134 μL, 1.05 mmol) or 1-CH_3isoQuin (140 μL, 1.05 mmol) were added dropwise. After the addition of 8-ClQuin or 1-CH_3isoQuin, a yellowish or brownish milky suspension was formed, respectively, and then the suspensions were sonicated for 10 min. Reactions were slowly concentrated until half of the volume under vacuum yielding a brownish (**4**) or pinkish (**5**) crystalline powder which was filtered and washed with 20 mL of milliQ water to remove the excess of KI. Then, the powders were dried under vacuum for 1 h.

{[CuI(8-ClQuin)]·8-ClQuin}$_2$ (**4**). Yield: 244 mg (90%). Anal. Calc. for $C_{27}H_{18}N_3Cl_2I_2Cu_2$ (1037.33 g mol^{-1}): C, 41.68; H, 2.53; N, 5.40%. Found: C, 41.54; H, 2.48; N 5.22%. FTIR-ATR (wavenumber, cm^{-1}): 3103(w) - 3001(w) [υ(C–H)]$_{ar}$, 2942(w), 1938(w), 1874(w), 1806(w), 1729(w), 1611(w), 1592(m) [υ(C═C/C═N)], 1490(m), 1460(m) [υ(C═C/C═N)], 1422(m) [δ(C═C/C═N)], 1381(m) [δ(C═C/C═N)], 1361(sh), 1306(m), 1242(w), 1215(m), 1202(sh), 1160 (w), 1147(m), 1134(w), 1065(m) [δ(C–H)]$_{ar}$, 1045(w), 1029(w), 986(m) [δ(C–H)]$_{ip}$, 976(s) [δ(C–H)]$_{ip}$, 954(sh), 902(m), 850(w), 818(s) [δ(C–H)]$_{oop}$, 807(m) [υ(C–Cl)], 783(s) [δ(C–H)]$_{oop}$, 776(s) [δ(C–H)]$_{oop}$, 758(s) [δ(C–H)]$_{oop}$, 677(m), 656(m), 625(w), 543(m). ^{1}H NMR (400 MHz; ACN-d_3; 298 K): δ = 8.85 [1H, dd, ^3J = 4.2 Hz, ^4J = 1.7 Hz, *o-H*$_{py}$], 8.25 [1H, dd, ^3J = 8.3 Hz, ^4J = 1.7 Hz, *o-H*$_{Cl}$], 7.79 [1H, dd, ^3J = 8.2 Hz, ^4J = 1.3 Hz, *p-H*$_{py}$], 7.76 [1H, dd, ^3J = 7.5 Hz, ^4J = 1.3 Hz, *p-H*$_{Cl}$], 7.46 [1H, dd, ^3J = 8.3 Hz, ^3J = 4.2 Hz, *m-H*$_{py}$], 7.41 [1H, dd, ^3J = 8.2 Hz, ^3J = 7.6 Hz, *m-H*$_{Cl}$].

[CuI(1-CH_3isoQuin)] (**5**). Yield: 208 mg (83%). Anal. Calc. for $C_{20}H_{18}N_2ICu$ (476.80 g mol^{-1}): C, 50.38; H, 3.80; N, 5.88%. Found: C, 50.21; H, 3.64; N 5.72%. FTIR-ATR (wavenumber, cm^{-1}): 3054(w) [υ(C–H)]$_{ar}$, 3014(w) [υ(C–H)]$_{ar}$, 2976(w) [υ(C–H)]$_{al}$, 1624(w), 1597 (w), 1562(m) [υ(C═C/C═N)], 1504(m) [υ(C═C/C═N)], 1460(w), 1431(w), 1419(w) [δ(C═C/C═N)], 1392(m) [δ(C═C/C═N)], 1369 (m), 1331(m), 1271(w), 1246(m), 1203(w), 1165(w), 1144(w), 1024 (w), 984(w), 960(w), 868(m) [δ(C–H)]$_{ip}$, 820(s) [δ(C–H)]$_{oop}$, 777(m) [δ(C–H)]$_{oop}$, 744(s) [δ(C–H)]$_{oop}$, 712(m), 642(m), 579(m), 538(m). ^{1}H NMR (400 MHz; $CDCl_3$; 298 K): δ = 8.23 [1H, d, ^3J = 5.9 Hz, *o-H*$_{py}$ (H_1)], 8.05 [1H, ddd, ^3J = 8.3 Hz, ^4J = 2.1 Hz, ^5J = 0.9 Hz, (H_6)], 7.74 [1H, d, ^3J = 7.5 Hz, (H_3)], 7.60 [1H, ddd, ^3J = 8.2 Hz, ^3J = 6.9 Hz, ^4J = 1.3 Hz, (H_4)], 7.51 [1H, ddd, ^3J = 8.3 Hz, ^3J = 6.9 Hz, ^4J = 1.4 Hz, (H_5)], 7.46 [1H, d, ^3J = 5.9 Hz, *m-H*$_{py}$ (H_2)], 2.82 [3H, s, –CH_3 (H_7)]. See S.I.: Fig. S17.

2.4. X-ray crystallographic data and structural analysis

Yellow (**1** and **4**), colorless (**2** and **3**), or red (**5**) prism-like specimens were used for the X-ray crystallographic analysis. The X-ray intensity data were measured on a D8 Venture system equipped with a multilayer

monochromator and a Mo microfocus. For **1**–**5**, the frames were integrated with the Bruker SAINT software package, using a narrow-frame algorithm. The integration of the data with a 0.70 Å resolution gave an average redundancy of 1.000 (**1** and **4**), 11.215 (**2**), 9.349 (**3**) or 9.457 (**5**), completeness of 99.4% (**1**), 99.5% (**2**), 99.8% (**3**), 99.9% (**5**) and 99.7% (**4**), an R_{sig} of 2.06% (**1**), 1.66% (**2**), 1.96% (**3**), 1.86% (**4**) or 8.78% (**5**) and from which 2433 (93.29%, **1**), 3206 (96.45%, **2**), 6564 (99.59%, **3**), 5203 (98.02%, **4**), or 1689 (61.04%, **5**) independent reflections were greater than $2\sigma(|F|^2)$.

The structures were solved and refined using the Bruker SHELXTL Software Package (version-2018/3) [26]. For **1**–**5**, the final cell constants and volume are based upon the refinement of the XYZ-centroids of reflections above 20 σ(I). Data were corrected for absorption effects using the multi-scan method (SADABS). Crystal data and relevant details of structure refinement for compounds **1**–**5** are reported in Tables 1 and 2.

The geometry evaluation of the Cu(I) in the five complexes was performed using version 2.1 of SHAPE [27] software, which is based on the low continuous-shape measure (CShM) value *S* [28]. The *S* value is a generalizable structural descriptor, to quantitatively evaluate distortion in terms of symmetry and distance from any ideal geometry. The corresponding atom coordinates were directly extracted from.cif data and *S* values were computed for any potential geometric accommodation within the corresponding coordination number. The ideal geometry presenting the lowest *S* value is then used to assign the coordination of Cu. Complete information about the crystal structure and molecular geometry is available in.cif format and deposited in the CCDC. CCDC numbers 2304580 (**1**), 2304582 (**2**), 2304581 (**3**), 2304579 (**4**), and 2304578 (**5**) contain the supplementary data of this paper. Molecular graphics were generated using Mercury (version 4.3.1) [29] with POV-Ray Package (version 3.7) [30]. Color codes for molecular graphics: light slate blue (N), light green (Cl), dark magenta (I), suva grey (C), white (H), red-orange (Cu) and red (O).

Table 1
X-ray crystallographic data of complexes **1**–**3**.

	1	2	3
Empirical formula	$C_6H_6N_2OICu$	$C_8H_9N_3OICu$	$C_{44}H_{36}N_4I_4Cu_4$
Formula weigh	312.57	353.62	1382.53
T (K)	100(2)	100(2)	100(2)
Wavelength (Å)	0.71073	0.71073	0.71073
System, space group	Monoclinic, $P2_1/c$	Triclinic, P-1	Monoclinic, $C2/c$
Unit cell dimensions			
a (Å)	13.4495(13)	4.01960(10)	20.9184(9)
b (Å)	4.0804(4)	9.5489(4)	13.6718(5)
c (Å)	16.5443(2)	14.2103(6)	17.4825(7)
α (°)	90	99.4590(10)	90
β (°)	109.601(4)	91.6200(10)	120.2520(10)
γ (°)	90	98.6280(10)	90
V (Å^3)	855.33(15)	531.14(10)	4319.0(3)
Z	4	2	4
*D*calc (g cm^3)	2.427	2.211	2.126
μ (mm^{-1})	6.105	4.932	4.839
F(000)	584	336	2624
Crystal size (mm^3)	0.192 × 0.056 × 0.035	0.248 × 0.104 × 0.029	0.417 × 0.326 × 0.297
hkl ranges	$-19 \le h \le 18$ $0 \le k \le 5$ $0 \le l \le 23$	$-5 \le h \le 5$ $-13 \le k \le 13$ $-20 \le l \le 20$	$-29 \le h \le 29$ $-19 \le k \le 19$ $-24 \le l \le 24$
2θ range (°)	2.568 to 30.590	2.189 to 30.825	1.943 to 30.538
Reflections collected/ unique/[R_{int}]	2608/2608/ 0.0343	37279/3324/ 0.0317	61617/6591/ 0.0376
Completeness to θ (%)	99.2	99.9	99.7
Absorption Correction	Semi-empirical	Semi-empirical	Semi-empirical
Max. and min. transmis.	0.7461 and 0.5960	0.7461 and 0.5542	0.7461 and 0.3555
Refinement method	Full matrix least-squares on $\|F\|^2$	Full matrix least-squares on $\|F\|^2$	Full matrix least-squares on $\|F\|^2$
Data/restrains/ parameters	2608/2/100	3324/0/128	6591/0/253
Goodness of fit (GOF) on $\|F\|^2$	1.202	1.093	1.444
Final *R* indices [$I > 2\sigma(I)$]	$R_1 = 0.0350$, $wR_2 = 0.0901$	$R_1 = 0.0115$, $wR_2 = 0.0279$	$R_1 = 0.0190$, $wR_2 = 0.0556$
R indices (all data)	$R_1 = 0.0374$ $wR_2 = 0.0911$	$R_1 = 0.0132$, $wR_2 = 0.0282$	$R_1 = 0.0191$, $wR_2 = 0.0557$
Extinction coefficient	n/a	n/a	n/a
Largest. Diff. peak and hole (e Å^{-3})	2.332 and −1.776	0.506 and −0.522	0.488 and −0.967

Table 2
X-ray crystallographic data of complexes **4** and **5**.

	4	5
Empirical formula	$C_{36}H_{26}Cl_4N_4I_2Cu_2$	$C_{20}H_{18}N_2ICu$
Formula weigh	1037.29	476.80
T (K)	100(2)	100(2)
Wavelength (Å)	0.71073	0.71073
System, space group	Triclinic, P-1	Monoclinic, $C2/c$
Unit cell dimensions		
a (Å)	8.7802(7)	12.5063(16)
b (Å)	9.2507(8)	8.2735(11)
c (Å)	11.3802(10)	18.019(2)
α (°)	95.242(3)	90
β (°)	97.437(3)	103.470(4)
γ (°)	107.599(3)	90
V (Å^3)	865.29(13)	1813.2(4)
Z	1	4
*D*calc (g cm^3)	1.991	1.747
μ (mm^{-1})	3.356	2.910
F(000)	502	936
Crystal size (mm^3)	0.305 × 0.180 × 0.072	0.132 × 0.027 × 0.018
hkl ranges	$-12 \le h \le 12$ $-13 \le k \le 13$ $0 \le l \le 16$	$-13 \le h \le 17$ $-11 \le k \le 11$ $-25 \le l \le 25$
2θ range (°)	2.332 to 30.558	2.324 to 30.541
Reflections collected/ unique/[R_{int}]	5308/5308/0.0298	26168/2767/0.1425
Completeness to θ (%)	99.9	99.9
Absorption Correction	Semi-empirical	Semi-empirical
Max. and min. transmis.	0.7461 and 0.5684	0.7461 and 0.4672
Refinement method	Full matrix least-squares on $\|F\|^2$	Full matrix least-squares on $\|F\|^2$
Data/restrains/parameters	5308/1/205	2767/0/111
Goodness of fit (GOF) on $\|F\|^2$	1.097	1.055
Final *R* indices [$I > 2\sigma(I)$]	$R_1 = 0.0567$, $wR_2 = 0.1448$	$R_1 = 0.0578$, $wR_2 = 0.1000$
R indices (all data)	$R_1 = 0.0573$, $wR_2 = 0.1452$	$R_1 = 0.1322$ $wR_2 = 0.1270$
Extinction coefficient	n/a	n/a
Largest. Diff. peak and hole (e Å^{-3})	4.430 and −2.278	1.185 and −1.504

2.5. Computational details

Geometry optimizations were conducted starting from the X-ray crystallographic data. All DFT calculations were performed with the Gaussian16 package, version B.01 [31]. Geometry optimizations were carried out without any geometrical constraint at the CAM-B3LYP density functional level [32]. We include the empirical dispersion correction D3 of Grimme for dispersive interactions [33]. The use of D3 was based on our previous experience in modeling coordination polymers in solid state [24]. All atoms were represented with the all-electron split-valence double-ζ def2SVP basis set [34,35], which also includes polarization functions. Test calculations with the larger all-electron split-valence triple-ζ def2TVP basis showed that basis set improvement does not imply important geometry differences but substantially increases the computational cost. Absorption spectra were obtained using the TD-DFT approach at the same CAM-B3LYP/def2SVP level of theory.

We included between 150 and 300 states, depending on the system, to account for all transitions in the UV–Vis region.

The different structures were represented starting from individual units to models including the vicinal units that interact with the central monomer, dimer, cubane, or polymer until the geometry of the complexes was similar to the X-Ray structures and the UV–Vis spectra were well reproduced. The *S* values of the optimized geometries were calculated and compared to the experimental structures to ensure minimal geometrical variations (S.I: Table S1).

For the sake of comparison, geometry optimization and LUMO energy calculations of the free ligands were conducted at the B3LYP density functional level [36], including empirical dispersion D3 [33] and all atoms were represented with the all-electron triple-ζ 6–311++G(3df, 3pd) basis set [37].

3. Results and discussion

In this contribution, we have performed the synthesis of five Cu(I)-halide based materials with five N-heterocyclic donor ligands (isn, nic, 3-phpy, 1-CH_3isoQuin and 8-ClQuin). All these reactions were performed in ACN at room temperature, except for 1-CH_3isoQuin and 8-ClQuin, which were synthesized in a mixture of a KI-saturated H_2O solution and ACN in a 1:0.3 ratio. The reactions containing the amide functionality have resulted in the formation of two staircase polymers with general formulas $[CuI(isn)]_n$ (**1**) and $\{[CuI(isn)]\cdot ACN\}_n$ (**2**), whereas the reaction with 3-phpy yielded the cubane $[CuI(3\text{-phpy})]_4$ (**3**). Finally, the incorporation of 8-ClQuin resulted in the rhomboid dimer $\{[CuI(8\text{-ClQuin})]\cdot 8\text{-ClQuin}\}_2$ (**4**) while 1-CH_3isoQuin formed the monomer [CuI(1-CH_3isoQuin)] (**5**). The synthesis of complexes **1**–**3** was assayed in a 1:2 (CuI:isn/nic/3-phpy) molar ratio, and the synthesis of **4** and **5** was performed using the 1:1 (CuI:8-ClQuin/1-CH_3isoQuin) molar ratio. For **1–3**, reactions proceeded as for the 1:1 M ratio whereas in the case of **4**, the introduction of an excess of 8-ClQuin provided better crystalline materials since, as revealed by the X-ray structure, an additional ligand is stacked within the dimers in a pillared arrangement. Hence, the synthesis of **1**–**3** was performed in 1:1 M ratio whereas **4** and **5** were obtained in the 1:2 M ratio.

From all the reported examples of Cu(I)-iodide complexes containing N-heteroaromatic ligands, it is inferred that reactions with the 1:1 M ratio in acetonitrile tend to arrange tetrameric cubanes whereas in a KI-saturated H_2O solution usually lead to the staircase polymer array [5]. The less sterically demanding ligands (isn, nic and 3-phpy) are suitable to arrange into the tetrameric cubane, so to compare between them the effect of the amide substituent, we performed the synthesis of **1**–**3** in ACN. As previously reported, the reaction with the unbiased ligand, the 3-phpy, resulted in the formation of the tetrameric cubane **3**. Instead, the reaction with either isn or nic resulted in the arrangement of the two staircase polymers **1** and **2**, and this result was achieved regardless of the molar ratio, since 1:2 reactions also led to the same arrangements. Then, considering that the two bulky ligands (8-ClQuin and 1-CH_3isoQuin) are not prone to form the tetrameric cubane, but there are reported examples of quinoline and derivatives forming staircase polymers, we performed the synthesis of both in a KI-saturated H_2O solution. Interestingly, the structural directing effect of the synthetic conditions was overcome by the effect of the substituents, and the dimer **4** and the monomer **5** were obtained. Therefore, these one-pot syntheses achieved a certain degree of control, which is the most important drawback to makes them feasible in the preparation of Cu(I)-iodide complexes.

Suitable crystals for the X-ray crystallographic analysis were grown *via* recrystallization of **1** (0.0101 g) or **2** (0.0081 g) in 5 mL of ACN at 75 °C and slow cooling down until 25 °C for 10 h. Suitable crystals **3** were obtained by slow evaporation of the mother liquors, whereas layering an ACN solution of 8-ClQuin or 1-CH_3isoQuin over a KI-saturated aqueous solution of CuI resulted in crystals **4** and **5**, respectively. The quality of single crystals **4** was poor but an X-ray diffraction analysis could be carried out and clearly revealed the structure of the complex.

General characterization. The five complexes were characterized by PXRD, elemental analysis (EA), FTIR-ATR and ^{1}H NMR spectroscopies, and single crystal X-ray diffraction. Besides, their photophysical properties in solid state were analyzed by UV–Vis and solid-state photoluminescence at room temperature.

The phase purity of the samples was confirmed by PXRD (S.I.: Figs. S1–S5). For better comparison, the FTIR-ATR of isn and nic ligands was added to the S.I.: Figs. S6–S7. The FTIR-ATR spectrum of complexes **1**–**5** can be observed in the S.I.: Figs. S8–S12. The υ(C═O) wavenumbers of amides bounded in region I (1800-1600 cm^{-1}) are sensitive to hydrogen bonds (HBs) and dipole-dipole interactions, whereas solvent exchange is better traced by changes in region II over 1570-1470 cm^{-1}. In addition, the formation of HBs is reflected as a downfield-shifted υ(N–H) vibration [38]. In complexes **1** and **2** both symmetric and asymmetric [υ(N–H)] vibrations suffer an upfield shift of 52 cm^{-1} and 37 cm^{-1} (**1**) or 49 cm^{-1} and 27 cm^{-1} (**2**), respectively, ascribed to a change in the assembly of the amide functionalities (S.I.: Figs. S6–S9). Additional bands from the ν[C═C/C═N] vibrations from isn and nic appears between 1379 and 1113 cm^{-1} [39]. Then, bands at 2287 and 2256 cm^{-1} attributable to the presence of ACN molecules [40] were also identified in the spectrum of **2**. This band corresponds to a mixture of [δ(C–H)+υ(C–C)] vibrational modes while the less energetic band belongs to the symmetric [υ(C≡N)] vibration [41]. Besides, symmetric [δ(C–H)$_3$] at 1358 and [υ(C–C)] at 924 cm^{-1} in **2**, [υ(C═C/C═N)] from aromatic rings in **3**–**5** (S.I.: Figs. S10–S12) as well as [υ(C–Cl)] vibration [42] at 807 cm^{-1} in **4** have been assigned (S.I.: Fig. S11). In addition, the fingerprint region of both **4** and **5** show the characteristic double bands between 820 and 699 cm^{-1} of the monosubstituted aromatic rings. Further identification of vibrational modes [43,44] can be found in the experimental details.

^{1}H NMR spectra of **1**–**5** were performed in ACN-d_3 at 298K (S.I.: Figs. S13–S17). The signal corresponding to the o-*H* aromatic protons appeared at 8.70 (**1**), 8.97 (**2**), 8.85 (**3** and **4**), and 8.23 (**5**) ppm. The most downfield-shifted signal in **2** agrees with the presence of the carbonyl group in *ortho* position with respect to the *H* atom. The remaining aromatic signals from pyridyl and phenyl rings can be found between 8.69 and 7.41 ppm. Besides, the protons of the amide functionalities from the –NH_2 moiety in **1** and **2** emerged between 6.10 and 6.90 ppm. The partial double bond character of the C–N bond in amides hinders free rotation i.e. with an energy barrier of 12.9 kcal/mol in nic or 14.1 kcal/mol in isn [45]. The rotation of both amide functional groups is affected by steric repulsion between the amide N-H_{anti} proton and an H atom from the pyridyl ring. Besides, resonance effects within the aromatic ring of isn and nic ligands distribute positive charge over the three carbon atoms in nic, while two *m*-H and the *N* atom are affected in isn. This less favorable delocalization in isn is reflected as a less stabilization and therefore, the double bond character in isn is decreased. This can be confirmed by the longer C–N bond length of isn (1.364(8) Å) with respect to nic (1.333(1) Å), which reflects a less double bond character. Despite isn having a higher rotational barrier, it presents a lesser double bond character by delocalization [45].

Molecular and supramolecular structures of $[CuI(isn)]_n$ (**1**) and $\{[CuI(nic)]\cdot ACN\}_n$ (2)

Complex **1** crystallized in the Monoclinic, $P2_1/c$, whereas **2** crystallized in the Triclinic, P-1 space groups and both accommodate double-stranded staircase 1D polymeric structures along *a* or *b* axis, respectively. The Cu(I) centers display $[CuI_3N]$ *cores* bearing slightly distorted tetrahedral geometries with *S* values of 1.569 (**1**) and 1.512 (**2**) and isn (Fig. 1a) or nic (Fig. 1b) monodentate ligands.

Cu···Cu distances evince the presence of cuprophilic interactions, Cu1···Cu1 2.824(1) Å in **1** or Cu1···Cu1 2.7176(3) Å and Cu1···Cu1 2.7747(3) Å in **2**. Bond lengths, angles, and cuprophilic interactions are within the range of similar double-stranded staircase 1D polymeric

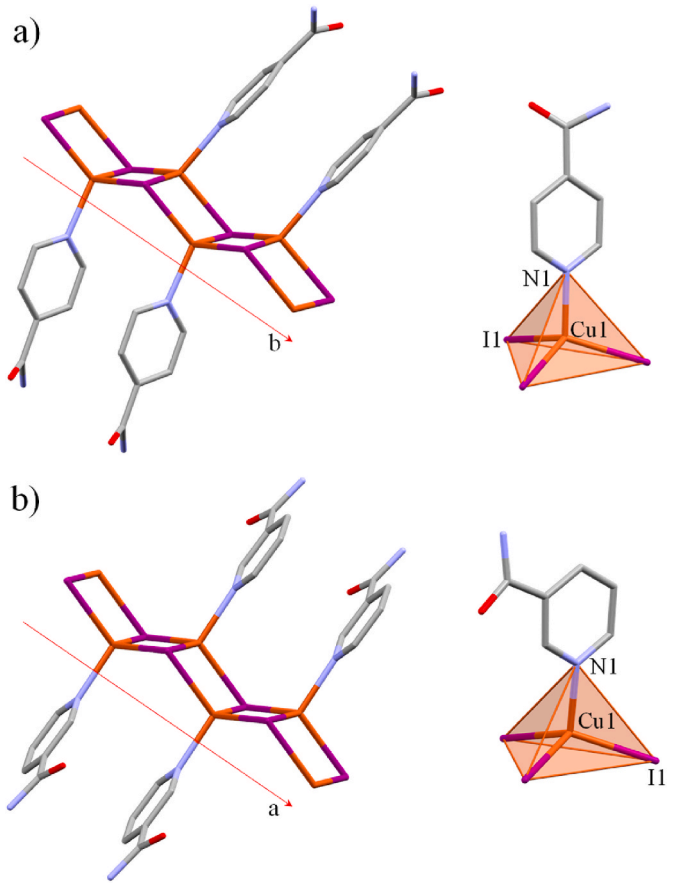

Fig. 1. Molecular structure of complexes (a) **1** and (b) **2.** In detail, CuI_3N *cores* with the labelling scheme.

structures (Cu···Cu, 2.709(2)-2.7791(5) Å; Cu–N, 2.055 Å; 56.96(8)°-133.8(14)°) [46,47] (Tables 3 and 4).

Interestingly, the inclusion of acetonitrile molecules into the crystal structure of complex **2** allows to minimize rotation of the amide functional group by fixing the N-H_{anti} (C3–C4–C6–N2 torsion angle of 9.47°). Instead, the greater C4–C3–C6–N2 torsion angle of 32.43° in **1** is probably caused by the interaction of N-H_{anti} proton with an iodide atom from neighboring chains that are slipped to improve the packing of the polymeric chains. This increased planarity of nic could favor electronic delocalization within the aromatic ring.

The assembly of the structures of **1** and **2** is unavoidably directed by the amide···amide homosynthon that usually displays one of the strongest interaction patterns with stabilization energies up to −157 kJ/mol [48]. Therefore, amide synthon forms supramolecular straight chains along the [1 1 $\bar{2}$] direction (**1**) or zigzag chains along *c* axis (**2**), caused by the different positions of the amide functionalities. In the case of **1**, N-H_{anti} and *m*-H atoms interact with consecutive iodide atoms from the neighboring polymeric chains combined with C–H···O interactions between *o*-H and the carbonyl *O* atom (Fig. 2a), joining the supramolecular layers into a 3D net. The further expansion in **2** is set by tetrel bonds (TBs) between the methyl group of ACN and the carbonyl from nic as well as between the N-H_{anti} and the *N* atom from ACN (Fig. 2b). These ACN molecules act as a bridge between nic ligands by associating between themselves through C–H···N interactions (Fig. 2c). In addition, they are located within supramolecular channels of 40.35 $Å^3$ (Fig. 2d), representing 7.6% of the unit cell volume (calculated using a probe radius of 1.2 Å). These associations define the 3D supramolecular structure of **2**.

Typical TBs happen between an electrophilic region on a tetrel element (group 14) and a nucleophilic region in another atom. Since they are exacerbated for elements further down group 14, which are more electrophilic, the *C* atom usually needs to be attached to an electron-withdrawing group as nitrile, which polarizes it and decreases its electron density [49]. Hence, the more electropositive nature of this C atom facilitates its engagement, which can be further evaluated by two broadly employed straightforward parameters R (distance between C and the nucleophile) and θ (angle between the atom directly attached to the C atom, the C atom, and the nucleophile), where $2.8 < R < 3.2$ Å and θ ~ 180° stands for purely TB whereas θ ~ 110° corresponds to a linear C–H···acceptor (O/N/S) HB [41]. Thus, from a structural point of view, the interaction between ACN and the O atom from nic stands for a TB (Table 4).

Besides, structural features agree with the spectroscopic data. Despite both ligands are displaying analogous double head-to-head interactions, the N-H_{anti} differs in **1** by interacting with an *I* atom whereas in **2** it interacts with an *N* from an acetonitrile molecule, therefore disrupting the common pattern in the original structure of the ligands. Likewise, the carbonyl group in the complexes replaces the N–H···O interaction with a weak C–H···O interaction in **1** or a TB in **2**. Therefore, the shift of the corresponding ν(C═O) frequency in **1** is larger moving from a strong to an almost negligible interaction whereas the presence of TB in **2** reduces this shift. Thorough studies were reported on the distinct effect of TBs and HBs into vibrational modes, so this spectroscopic data can be supported by comparison with their structural features. Bending modes as symmetric CH_3 deformation are more sensitive to TB formation with a consequent increase in wavenumber (from 1375 cm^{-1} of free ACN to 1358 cm^{-1} in **2**), whereas stretching vibrations are less sensitive with red-shifted values (from 918 cm^{-1} of free ACN to 924 cm^{-1} in **2**).

Table 3
Bond lengths (Å), bond angles (°) and intermolecular interactions present in **1**.

Bond lengths			
Cu(1)–I(1)[a]1	2.5997(7)	Cu(1)–I(1)[a]2	2.6940(7)
Cu(1)–I(1)	2.6375(7)	Cu(1)–N(1)	2.023(4)
Bond Angles			
Cu(1)[a]1-I(1)-Cu(1)	91.0(2)	I(1)-Cu(1)-I(1)[a]1	113.76(3)
Cu(1)[a]1-I(1)-Cu(1)[a]2	100.84(2)	N(1)-Cu(1)-Cu(1)[a]1	118.15(12)
Cu(1)-I(1)-Cu(1)[a]2	63.956(19)	I(1)[a]2-Cu(1)-Cu(1)[a]1	124.77(4)
N(1)-Cu(1)-I(1)[a]2	115.45(12)	I(1)-Cu(1)-Cu(1)[a]1	56.73(3)
N(1)-Cu(1)-I(1)	107.62(12)	I(1)[a]1-Cu(1)-Cu(1)[a]1	57.049(16)
I(1)[a]2-Cu(1)-I(1)	116.99(3)	N(1)-Cu(1)-Cu(1)[a]2	133.21(13)
N(1)-Cu(1)-I(1)[a]1	101.04(12)	I(1)[a]2-Cu(1)-Cu(1)[a]2	58.017(17)
I(1)[a]2-Cu(1)-I(1)[a]1	100.84(2)	I(1)-Cu(1)-Cu(1)[a]2	58.99(3)

Intermolecular Interactions	H···A (Å)	D···A (Å)	D-H (Å)	>D-H···A (°)
N(2)-H(2A)···O(1)	1.980	2.86(1)	0.880	178
N(2)-H(2B)···I(1)	2.9151	3.764(6)	0.880	163
C(4)–H(4)···I(1)	3.1231	4.067(5)	0.951	172

[a] 1 -x,y+1/2,-z+3/2 #2 -x,y-1/2,-z+3/2.

Molecular and supramolecular structure of $[CuI(3\text{-phpy})]_4$ (3)

Complex **3** crystallized in the Monoclinic, *C*2/*c* space group and is composed of tetranuclear Cu_4I_4 cubane-like clusters with four monodentate 3-phpy ligands that present torsion angles (χ) of 52.47° and 46.02° (Fig. 3a). Each Cu(I) displays a [CuI_3N] *core* (Fig. 3b) and exhibits a slightly distorted tetrahedral geometry with *S* values of 1.990 (Cu1A) and 1.790 (Cu2A).

Considering that the sum of the van der Waals radii of Cu(I) is 2.8 Å, Cu···Cu distances evidence the presence of cuprophilic interactions [50] being Cu1A···Cu1A 2.6174(7) Å, Cu2A···Cu2A 2.6141(4) Å, Cu1A···Cu2A 2.7181(5) Å and Cu1A···Cu2A 2.6539(4) Å. These values are in the range of similar Cu_4I_4 cubane clusters with pyridine derivatives (2.604(1)-2.810(2) Å) [51–53]. The absence of significant hydrogen bond donors, in combination with the torsioned aromatic rings, results in discrete molecules from which only two weak C–H···I interactions are found (Fig. 3c–Table 5).

Table 4
Bond lengths (Å), bond angles (°) and intermolecular interactions present in **2**.

Bond lengths				
I(1)–Cu(1)	2.63072(19)	I(1)–Cu(1) #2	2.66032(16)	
I(1)–Cu(1) #1	2.65894(16)	Cu(1)–N(1)	2.0529(9)	
Bond Angles				
Cu(1)-I(1)-Cu(1)#1	63.274(6)	N(1)-Cu(1)-Cu(1)#2	124.51(3)	
Cu(1)-I(1)-Cu(1)#2	61.810(5)	I(1)-Cu(1)-Cu(1)#2	59.630(5)	
Cu(1)#1-I(1)-Cu(1)#2	98.168(5)	I(1)#1-Cu(1)-Cu(1)#2	125.057(8)	
N(1)-Cu(1)-I(1)	106.30(3)	I(1)#2-Cu(1)-Cu(1)#2	58.560(6)	
N(1)-Cu(1)-I(1)#1	109.45(3)	N(1)-Cu(1)-Cu(1)#1	125.82(3)	
I(1)-Cu(1)-I(1)#1	116.726(5)	I(1)-Cu(1)-Cu(1)#1	58.859(5)	
N(1)-Cu(1)-I(1)#2	107.53(3)	I(1)#1-Cu(1)-Cu(1)#1	57.867(5)	
I(1)-Cu(1)-I(1)#2	118.190(5)	I(1)#2-Cu(1)-Cu(1)#1	125.733(8)	
I(1)#1-Cu(1)-I(1)#2	98.167(5)	Cu(1)#2-Cu(1)-Cu(1)#1	94.077(8)	
Intermolecular Interactions	H···A (Å)	D···A (Å)	D-H (Å)	>D-H···A (°)
N(2)-H(2A)···O(1)	2.06	2.9362(13)	0.880	174
C(17)–H(17)···O(9)	2.23	3.0834(16)	0.880	164
C(8)-H(8B)···O(1)	2.5064	3.474(1)	0.980	169
N(2)-H(2B)···N(3)	2.227	3.083(2)	0.880	164
O(1)···C(8)	R = 3.064(2) Å		θ = 174.9(9)°	

#1 -x-1,-y+1,-z+1 #2 -x,-y+1,-z+1.

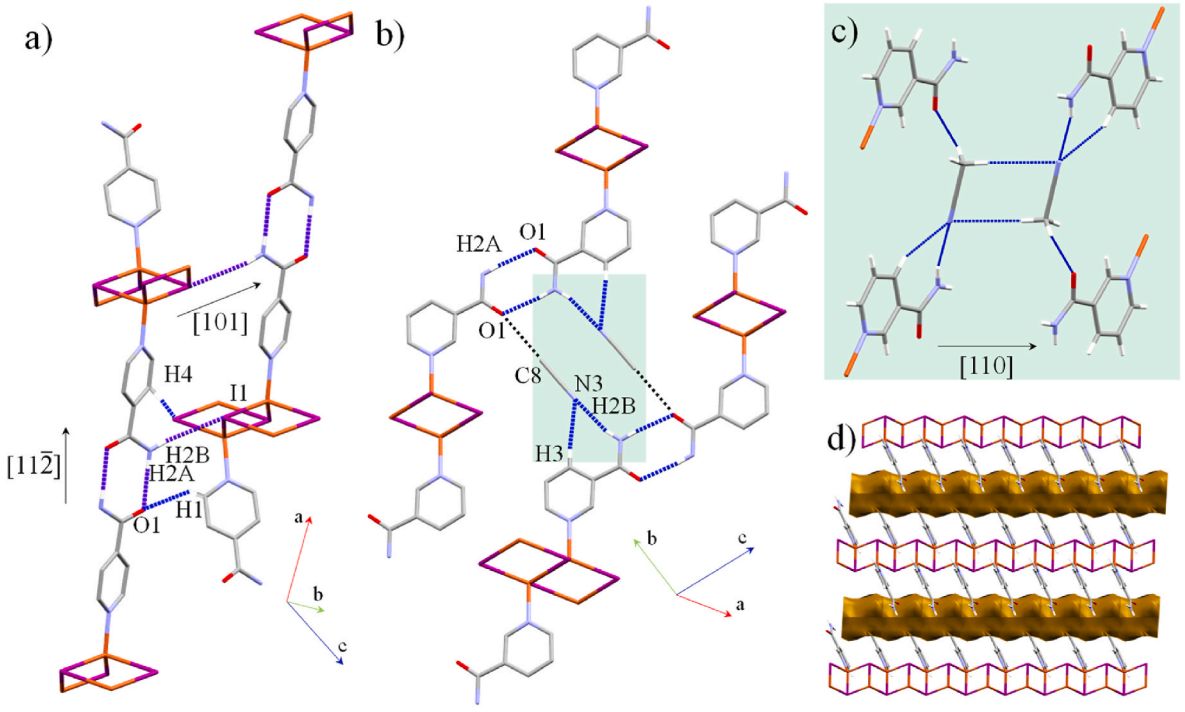

Fig. 2. Supramolecular structure of complexes **1** and **2**. (a) amide···amide, amide···I and C–H···O interactions in **1**. (b) Amide···amide and amide···ACN interactions as well as C···O TBs, highlighted with dotted dark lines, in **2**. (c) Association between nic and ACN and ACN molecules themselves. (d) Supramolecular channels of **3**.

Molecular and supramolecular structure of {[CuI(8-ClQuin)]·8-ClQuin}$_2$ (4)

Complex **4** crystallizes in the Triclinic, P-1 space group and it is composed of rhomboid Cu_2I_2 dimers with two additional 8-ClQuin ligands (Fig. 4a). The *S* values of the Cu(I) centers suggest a better fitting to a trigonal planar geometry rather than the four coordinated (*S* = 1.132 for trigonal planar (TP-3) and *S* = 3.008 for vacant trigonal bipyramid (vTBPY-4)) and define a [$Cu_2I_2N_2$] *core*, in which chlorine atom is capping one available coordination site by Cu···Cl interaction (Cu1···Cl1, 2.599(2) Å, Table 6). Therefore, the 8-ClQuin ligands simultaneously force the arrangement of tricoordinate Cu(I) centers and the slight pyramidalization of the geometry being the Cu(I) center 0.288 Å out of the plane formed by the coordinated donor atoms (N1–I1–I1) (Fig. 4b). Usually, 2-substituted ligands promote longer Cu···Cu distances than 3- and 4-substituted, due to steric effects but Cl substituent behaves more like a chelating ligand through the attractive Cl···Cu interaction. Besides, bulky or chelate ligands usually promote a closing of the L-Cu-L' angle (L = ligand) and the consequent opening of the I–Cu–I angle, which in **4** is of 120.57°, larger if compared to previously reported complexes ranging between 110.57(2)° and 114.92(1)° [21]. This is reflected as a significantly short Cu···Cu distance of 2.5595(12) Å, compared to analogous complexes which display values around 2.607 (2) Å and 2.664(1) Å [21].

The structure of **4** is assembled into stacked layers of dimers and free 8-ClQuin molecules through complementary π···π interactions in an alternated manner (8-ClQuin···dimer···dimer···8-ClQuin). Dimers and free 8-ClQuin associate between themselves by triple π···π stackings, featuring a pyridyl-pyridyl (Cg1···Cg3), pyridyl-phenyl (Cg1···Cg2 and Cg2···Cg3) and phenyl-phenyl (Cg2···Cg4) fashion along [011] direction

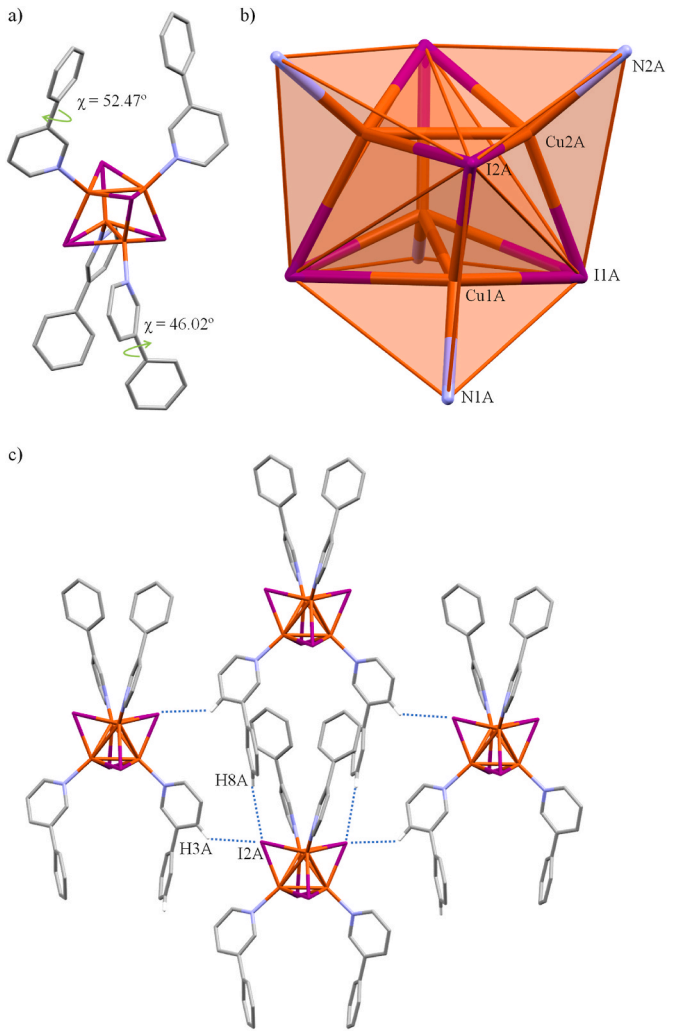

Fig. 3. (a) Molecular structure of **3** highlighting the torsion angle between phenyl and pyridyl rings. (b) Inset of the cubane-like arrangement with labeling scheme. Hydrogen atoms have been omitted for clarity. (c) Supramolecular assembly of **3**. Only hydrogen atoms involved in the intermolecular interactions are shown.

(Fig. 5a), and designing 2D layers within the (100) plane (Fig. 5b).

Molecular and supramolecular structure of [CuI(1-CH_3isoQuin$)_2$] (5)

Complex **5** crystallizes in the Monoclinic *C2/c* space group, and it contains two monodentate 1-CH_3isoQuin ligands in a [CuN_2I] *core* with a slightly distorted trigonal planar geometry ($S = 0.830$) (TP-3 = 0.830), exhibiting angles of 137.9(3)° and 111.06(14)°, forced by the steric hindrance between the ligands. Indeed, the Cu(I) center is perfectly accommodated on the plane defined by the coordinated atoms (Fig. 6a). The 1-CH_3isoQuin ligands are arranged almost perpendicular with a (C9–N1–N1–C9) torsion angle of 86.0(6)° probably guided by the bulky methyl groups in *ortho* position.

This almost perpendicular disposition of the 1-CH_3isoQuin ligands forces the monomeric units to assemble into 2D layers through double π···π interactions between pyridyl-phenyl rings (Cg1···Cg2) and *vice versa* (Fig. 6b). The monomeric units are further associated by double C4–H4···I1 interactions between the *o*-H from the pyridyl rings and the iodide atom along *c* axis (Fig. 6c). Selected distances and angles are listed in Table 7.

Table 5
Bond lengths (Å), bond angles (°) and intermolecular interactions present in **3**.

Bond lengths			
I(1A)-Cu(1A)	2.6436(3)	I(2A)-Cu(2A)	2.6910(3)
I(1A)-Cu(2A)	2.6608(3)	I(2A)-Cu(2A)[a]1	2.7260(3)
I(1A)-Cu(1A)[a]1	2.7882(3)	Cu(1A)-N(1A)	2.0280(18)
I(2A)-Cu(1A)	2.6461(3)		
Bond Angles			
Cu(1A)-I(1A)-Cu(2A)	60.040(8)	I(2A)-Cu(1A)-I(1A)[a]1	110.076(10)
Cu(1A)-I(1A)-Cu(1A)[a]1	57.541(11)	Cu(2A)-Cu(1A)-I(1A)[a]1	107.379(11)
Cu(2A)-I(1A)-Cu(1A)[a]1	59.791(8)	Cu(2A)[a]1-Cu(1A)-I(1A)[a]1	57.777(8)
Cu(1A)-I(2A)-Cu(2A)	59.631(8)	N(2A)-Cu(2A)-Cu(2A)[a]1	137.88(5)
Cu(1A)-I(2A)-Cu(2A)[a]1	60.769(8)	N(2A)-Cu(2A)-Cu(1A)	149.93(5)
Cu(2A)-I(2A)-Cu(2A)[a]1	57.701(10)	Cu(2A)[a]1-Cu(2A)-Cu(1A)	62.120(10)
N(1A)-Cu(1A)-Cu(1A)[a]1	135.20(5)	N(2A)-Cu(2A)-I(1A)	109.52(5)
N(1A)-Cu(1A)-I(1A)	107.88(5)	Cu(2A)[a]1-Cu(2A)-I(1A)	112.504(6)
Cu(1A)[a]1-Cu(1A)-I(1A)	64.005(11)	Cu(1A)-Cu(2A)-I(1A)	59.659(8)
N(1A)-Cu(1A)-I(2A)	111.19(5)	N(2A)-Cu(2A)-I(2A)	106.02(5)
Cu(1A)[a]1-Cu(1A)-I(2A)	112.434(6)	Cu(2A)[a]1-Cu(2A)-I(2A)	61.823(11)
I(1A)-Cu(1A)-I(2A)	111.852(10)	Cu(1A)-Cu(2A)-I(2A)	59.344(9)
N(1A)-Cu(1A)-Cu(2A)	155.56(5)	I(1A)-Cu(2A)-I(2A)	109.910(10)
Cu(1A)[a]1-Cu(1A)-Cu(2A)	62.077(10)	N(2A)-Cu(2A)-Cu(1A)[a]1	145.72(5)
I(1A)-Cu(1A)-Cu(2A)	60.301(9)	Cu(2A)[a]1-Cu(2A)-Cu(1A)[a]1	59.662(9)
I(2A)-Cu(1A)-Cu(2A)	61.026(9)	Cu(1A)-Cu(2A)-Cu(1A)[a]1	58.303(13)
N(1A)-Cu(1A)-Cu(2A)[a]1	141.46(5)	I(1A)-Cu(2A)-Cu(1A)[a]1	62.433(9)
Cu(1A)[a]1-Cu(1A)-Cu(2A)[a]1	59.623(9)	I(2A)-Cu(2A)-Cu(1A)[a]1	107.953(11)
I(1A)-Cu(1A)-Cu(2A)[a]1	109.768(11)	N(2A)-Cu(2A)-I(2A)[a]1	101.27(5)
I(2A)-Cu(1A)-Cu(2A)[a]1	61.070(9)	Cu(2A)[a]1-Cu(2A)-I(2A)[a]1	60.476(11)
Cu(2A)-Cu(1A)-Cu(2A)[a]1	58.220(12)	Cu(1A)-Cu(2A)-I(2A)[a]1	108.802(11)
N(1A)-Cu(1A)-I(1A)[a]1	97.06(5)	I(1A)-Cu(2A)-I(2A)[a]1	111.553(11)
Cu(1A)[a]1-Cu(1A)-I(1A)[a]1	58.456(10)	I(2A)-Cu(2A)-I(2A)[a]1	117.848(10)
I(1A)-Cu(1A)-I(1A)[a]1	117.785(11)	Cu(1A)[a]1-Cu(2A)-I(2A)[a]1	58.161(9)
Torsion Angles			
C11(A)-C(6A)-C(4A)-C(5A)	52.5(3)	C16(A)-C15(A)-C17(A)-C5(A)	46.02
Intermolecular Interactions	H···A (Å)	D···A (Å) D-H (Å)	>D-H···A (°)
C(8A)-H(8A)···I(2A)	3.1356	3.910(2) 0.930	141.9
C(3A)-H(3A)···I(2A)	3.3269	3.891(3) 0.930	121.2

[a] 1 -x+1,y,-z+1/2.

3.1. Crystal engineering of tetracoordinate Cu(I)-iodide complexes

Considering the aforementioned tendency of Cu(I)-iodide systems to suffer molecular rearrangements after external stimuli, and the distortions displayed by complexes **1**–**5**, we performed a search in the CSD [54] to analyze distortions in the most common arrangements. Within the plethora of accessible architectures reported, we trimmed down the structural data to those structures bearing Cu(I)-iodide and monodentate pyridine derivative ligands (L) that should minimize geometric constraints from the ligands, assuming that only μ_3-iodine geometric restrictions are present in polynuclear complexes. This search has revealed that 80 examples (●) hold the polymeric 1D staircase chain [CuI(L)]$_n$, whereas 30 structures (◆) accommodate the cubane

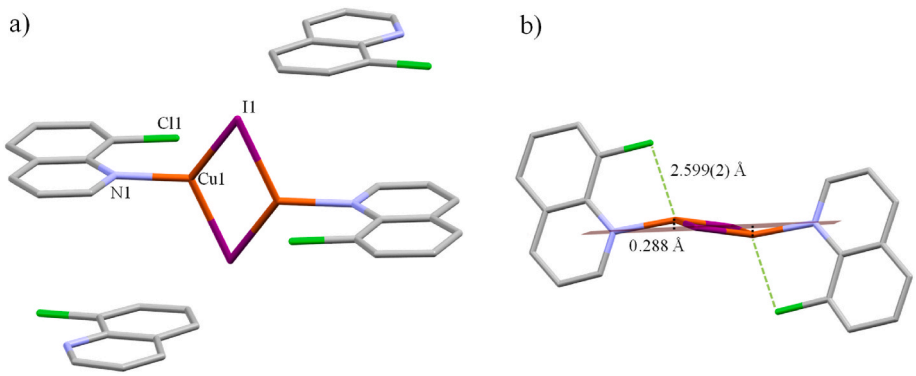

Fig. 4. (a) Molecular structure of **4**. (b) Highlighting of the Cu(I) out of N1–I1–I1 plane displacement towards Cl1 atom.

Table 6
Bond lengths (Å), bond angles (°) and intermolecular interactions present in **4**.

Bond lengths					
I(1)–Cu(1)	2.5732(7)		Cu(1)···Cu(1)#1		2.5595 (12)
I(1)–Cu(1)#1	2.5903(7)		Cu(1)···Cl(1)		2.5987 (17)
Cu(1)–N(1)	2.065(3)				
Bond Angles					
Cu(1)-I(1)-Cu(1)#1	59.43(2)		I(1)-Cu(1)-I(1)#1		120.57(2)
N(1)-Cu(1)-Cu(1) #1	158.90(11)		N(1)–Cu(1)···Cl(1)		79.98(11)
N(1)-Cu(1)-I(1)	118.55(11)		Cu(1)#1···Cu(1)···Cl(1)		120.75(5)
Cu(1)#1···Cu(1)–I (1)	60.62(3)		I(1)–Cu(1)···Cl(1)		110.84(4)
N(1)-Cu(1)-I(1)#1	116.56(11)		I(1)#1-Cu(1)···Cl(1)		98.73(4)
Cu(1)#1···Cu(1)–I (1)#1	59.95(3)				
Intermolecular Interactions	H···A (Å)		D···A (Å)	D-H (Å)	>D-H···A (°)
C15–H15···O9	2.318		3.229 (9)	0.950	160.4
C17–H17···O9	2.441		3.340 (10)	0.950	158.3
π interactions					
Cg(I)···Cg(J)	Cg···Cg[a]	α[b]	β, γ[c]	Cg(I)_Perp,Cg (J)_Perp[d]	Slippage[e]
Cg(1)···Cg(2)	3.692 (3)	1.2 (4)	23.7, 24.8	3.3514(15), 3.382(2)	1.484
Cg(1)···Cg(3)	3.725 (2)	2.3 (2)	22.3, 24.5	3.3903(15), 3.4463(18)	1.413
Cg(2)···Cg(2)	3.596 (3)	0	20.0, 20.0	3.379(2), 3.379(2)	1.230
Cg(2)···Cg(3)	3.704 (3)	3.2 (2)	19.3, 22.2	3.4297(18), 3.496(2)	1.224
Cg(2)···Cg(4)	3.707 (3)	4.2 (2)	15.9, 20.0	3.485(2), 3.5648(18)	1.016
Cg(3)···Cg(4)	3.679 (3)	1.3 (2)	24.1, 23.3	3.3788(18), 3.3576(18)	1.502
Cg(4)···Cg(4)	3.510 (3)	0	15.8, 15.8	3.3778(18), 3.3779(18)	0.954

#1 -x+1,-y,-z+1; [a]Cg···Cg = distance between ring centroids given in Å; [a]Cg···Cg = distance between ring centroids (Å); [b]α = dihedral angle between Planes I and J (°); [c]Offset angles: β = angle Cg(I)-Cg(J) and normal to plane I (°) and γ = angle Cg(I)-Cg(J) and normal to plane J (°) (β = γ, when α = 0); [d]Perpendicular distance (Å) of Cg(I) on plane J and perpendicular distance (Å) of Cg(J) on plane I (equal when α = 0); [e]Slippage = Horizontal displacement or slippage between Cg(I) and Cg(J) (equal for both centroids when α = 0). Cg(1) = N1–C1–C2–C3–C4–C9; Cg(2) = C4–C5–C6–C7–C8–C9; Cg(3) = N2–C10–C11–C12–C13–C18; Cg(4) = C13–C14–C15–C16–C17–C18.

tetrameric cluster $[Cu_4I_4(L)_4]$, 31 hits (◐) display the molecular rhomboid dimer $[Cu_2I_2(L)_n]$ (n = 1 or 2), and 22 hits (⬟) have a monomeric arrangement (Fig. 7) [54].

It is widespread knowledge that, from the geometric possibilities of tetracoordinate transition metal ions, those with d^8 electron configuration prefer square-planar geometry, whereas d^0 and d^{10} tend to be tetrahedral. Such a rule of thumb is ideal and usually intermediate geometries are found. In fact, previous studies on tetracoordinated Cu(II) and Pt(II) halide complexes show intermediate geometries between tetrahedron and square. A profound analysis of geometrical distortions of $[CuCl_4]^{2-}$ and $[CuBr_4]^{2-}$ structures evinced that the specific tetrahedral to square planar distortive mode that leads tetracoordinated species to interconvert from square to tetrahedron and *vice versa* fits the *spread* planarization route [55]. Besides, geometrical distortions of unit blocks, including $[Tl(Pb)X_4]^{2-}$ structures (X = Cl, Br) were previously detected for several thallium and lead chlorides and bromides [56–58]. Despite Cu(I) meeting the required d^{10} electron configuration which is one of the contributors to the tetrahedral geometry [59], Cu(I)-iodine complexes seem to follow a distinct pathway and should be considered as a particular case.

Hence, we decided to provide a shape map represented as a two-dimensional scatterplot of the two polyhedral that better fit, the tetrahedral (T-4) or the vacant trigonal bipyramidal (vTBPY-4) geometries (Fig. 7). Besides, *S* values for rhomboid dimers and monomers with the mentioned geometries are added.

The generated shape map displays that distortions are overtly accentuated for cubanes, which accommodate intermediate geometries with *S* values from (vTBPY-4 1.370; T-4 1.868) to (vTBPY-4 1.994; T-4 1.855) but bounded to a narrow range of distortions. Instead, stairstep polymers and rhomboid dimers better fit to a T-4 geometry, further from intermediates. Finally, monomeric arrangements should be sorted apart since despite presenting intermediate geometries all are guided by pincer trischelate ligands, which orientate the three coordinated *N* atoms [60], and thus, ligands themselves force the distortion. The *S* value calculations of tetracoordinate $[CuI_3N]$ *cores* for square (SP-4) and seesaw or sawhorse (SS-4) geometries gave high distortions with respect to T-4 and vTBPY-4, and therefore, we pose that $[CuI_3N]$ *cores* follow a *pyramidalization* or *umbrella* distortion conversion path [61].

The confined distortions in cubanes are probably induced by the cluster itself where bridging μ_3-iodine atoms force pyramidalization of tetrahedral geometry leading to distorted vTBPY-4 geometries but minimizing the accessible distortions in concert. Besides, these intermediate geometries instead of the preferred tetrahedral for the remaining arrangements could be triggered by cuprophilic interactions, which attract the Cu(I) centers to the center of the cubane and place them over the μ_3-iodines plane, thus favoring the vTBPY-4 geometry. It is also reflected that geometries between polymers and cubanes are the most similar, and this could allow easier interconversion between these arrays. Indeed, conversion between cubane and stair step polymers is commonly found [10,62].

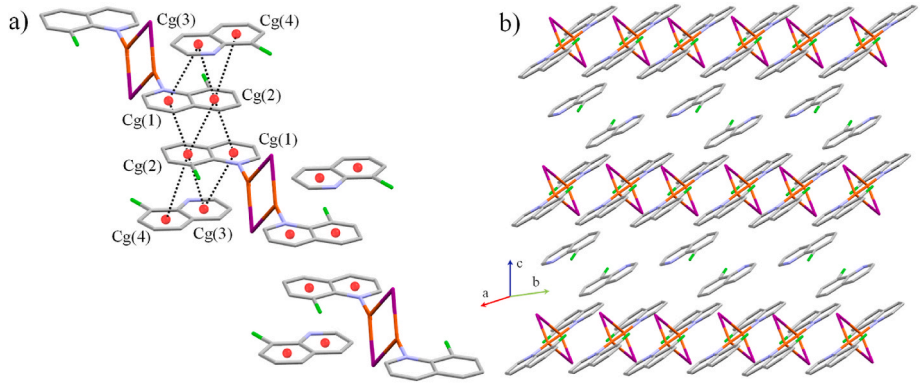

Fig. 5. (a) supramolecular assembly of 8-ClQuin throughout [011] direction supported by complementary π···π interactions. (b) Layered structure of **4** along (100) plane.

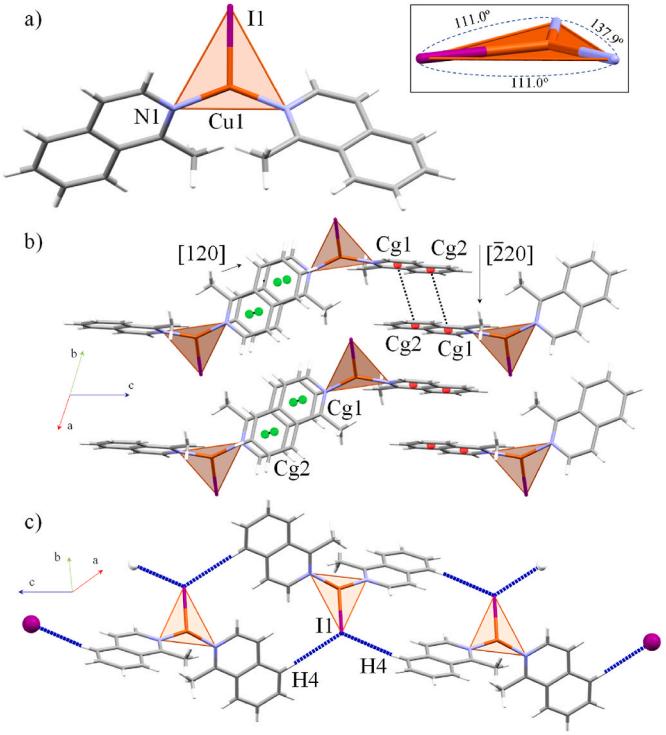

Fig. 6. Molecular structure (a) and supramolecular structure assembled by π···π (b) and C–H···I (c) interactions of **5**.

Table 7
Bond lengths, angles and intermolecular interactions in complex **5**.

Bond lengths					
I(1)–Cu(1)	2.5757 (13)	Cu(1)–N(1)#1			1.965(5)
Bond Angles					
N(1)-Cu(1)-N(1)#1	137.9(3)	N(1)#1-Cu(1)-I(1)			111.06 (14)
Intermolecular Interactions	H···A (Å)	D···A (Å)	D-H (Å)		>D-H···A (°)
C(4)–H(4)···I(1)	3.1195	4.061	0.950		171.29
π interactions					
Cg(I)···Cg(J)	Cg···Cg[a]	α[b]	β, γ[c]	Cg(I)_Perp, Cg(J)_Perp[d]	Slippage[e]
Cg(1)···Cg(2)	3.876(4)	2.2(3)	22.7, 22.4	3.585(2), 3.575(3)	1.496
Cg(1)···Cg(2)	3.703(4)	2.2(3)	15.4, 16.9	3.544(2), 3.570(3)	0.985
Cg(2)···Cg(1)	3.876(4)	2.2(3)	22.4, 22.7	3.576(3), 3.584(2)	1.476
Cg(2)···Cg(3)	3.704(4)	2.2(3)	16.9, 15.4	3.570(3), 3.544(2)	1.075

#1 -x+1,-y,-z+1; [a]Cg···Cg = distance between ring centroids given in Å; [a]Cg···Cg = distance between ring centroids (Å); [b]α = dihedral angle between Planes I and J (°); [c]Offset angles: β = angle Cg(I)-Cg(J) and normal to plane I (°) and γ = angle Cg(I)-Cg(J) and normal to plane J (°) (β = γ, when α = 0); [d]Perpendicular distance (Å) of Cg(I) on plane J and perpendicular distance (Å) of Cg(J) on plane I (equal when α = 0); [e]Slippage = Horizontal displacement or slippage between Cg(I) and Cg(J) (equal for both centroids when α = 0). Cg(1) = N1–C1–C2–C3–C8–C9; Cg(2) = C3–C4–C5–C6–C7–C8.

3.2. Photophysical properties: experimental and theoretical calculations

3.2.1. Solid-state UV–Vis and photoluminescence

Previously reported cases stand for intermolecular interaction modification [19] or isomeric conversion after grinding [13]. To avoid changes in the photophysical properties of the complexes upon the preparation of the samples for the UV–Vis and photoluminescence measurements [63], the PXRD patterns of the samples after grinding are provided in the S.I.: Figs. S1–S5. In addition, Fig. 8 provides a visual inset of the samples under UV irradiation before and after grinding, also suggesting no significant changes in the emission color. Besides, the potential thermochromic behavior associated with these materials is attributed to changes in the cuprophilic interactions, exhibited by those holding distances below the sum of the vdW radii of 2.8 Å (Table 8). Therefore, we provide an inset of the samples irradiated under the same conditions immersed in liquid nitrogen (Fig. 8). Upon cooling, samples **2** and **3** present changes in the emission color as would be expected considering that Cu···Cu distance is below 2.8 Å. Cubane arrangements are prone to present this behavior due to the enhancement of the emission from the LE band, instead, staircase polymers have less tendency since usually display longer distances [19].

Upon the UV–Vis radiation exposure at 298K, the samples **1**–**5** (Fig. 9) display broad absorption bands up to 500 (**1** and **4**), 450 (**2**), 400 (**3**), and 525 (**5**) nm, with absorption maxima at 415 (**1**), 325 (**2**), 275 (**3**), 380 (**4**), and 375 (**5**) nm. Complexes **2** and **5** have additional less intense bands from 450 to 700 nm (**2**) and 525–700 nm (**5**). These unstructured absorption spectra are usually related to charge transfer processes, which is in agreement with the reported excitation pathways for Cu(I)-iodide materials.

The emission spectra of complexes **1**, **2**, **3**, and **5** (Fig. 10) display broad bands with emission maxima ($\lambda_{em\text{-}max}$) at 529 (**1**), 479 (**2**), 552 (**3**), and 600 nm (**5**), and full width at half maximum (FWHM) values between 62.7 and 119.1 (Table 9). Instead, the emission spectrum of **4** displays well-defined bands with FWHM of 7.5 with the emission maxima at 413 nm. Interestingly, the spectra of **1**, **2**, and **5** display additional bands at 650 nm (**1**), 360 nm, and 550 nm (**2**), at 423 nm and up to 700

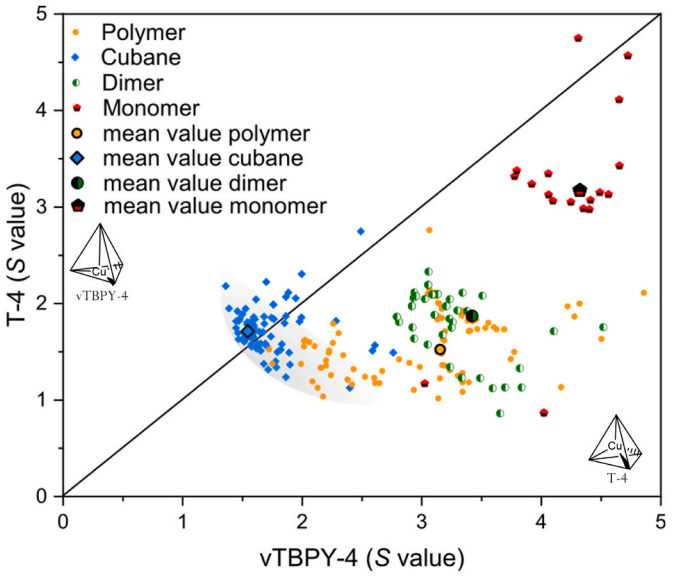

Fig. 7. Shape map of the tetracoordinated *cores* containing Cu(I)-iodide with pyridine derivatives bearing T-4 or vTBPY-4 geometries.

nm (**5**). Complexes **1**–**5** display emission within the range of the corresponding architectures with *N*-heteroaromatic donors. Staircase polymers usually exhibit emission between 530 and 630 nm, tetrameric cubanes between 555 and 625 nm, dimers between 466 and 620 nm, and monomers between 460 and 650 nm [6,54,64,65]. For the sake of comparison, some relevant parameters of the archetypal analogues with pyridine are reported in Table 9. The values of Stokes shifts are related to rigidity of the complexes and planarity of the ligands since planar molecules usually display small Stokes shifts. Thus, the reported complexes **1**–**3** display larger Stokes shifts compared to the pyridine analogues. Instead, complex **4** with a more rigid 8-ClQuin ligand show significantly small Stokes shift. This is in agreement with the energy of the HOMO from **4** which is of −6.3261 eV, whereas the LUMO is at −1.6207 eV. Thus, the LUMO from 8-ClQuin at −2.0493 eV provides an accessible low-lying MO triggering relaxation from coordinated 8-ClQuin to occluded 8-ClQuin ligand instead of returning to the Cu_2I_2 *core*. The CIE chromaticity diagram of complexes **1**–**5** (S.I.: Fig. S18) highlights the tunable emission of the complexes covering the whole range of the visible spectrum.

Interestingly, several studies for rhomboid dimers inferred that the incorporation of ligands with higher LUMO energies results in more energetic emission bands [21]. The calculated LUMO energies are −1.9870 eV for isn, −1.7720 eV for nic, −1.3987 eV for 3-phpy, −2.0493 eV for 8-ClQuin, and −1.6912 eV for 1-CH_3isoQuin. Besides, reported data provides a LUMO energy of 0.4890 eV for pyridine [67]. Considering our results, it seems that staircase polymers follows the same trend as rhomboid dimers, since LUMO energies of the ligands are

Table 8
Selected Cu···Cu distances (in Å) of complexes **1**–**5**.

1	2.824(1)	**4**	2.5595(12)
2	2.7176(3), 2.7747(3)	**5**	7.498
3	2.6174(7), 2.6141(4), 2.7181(5), 2.6539(4)		

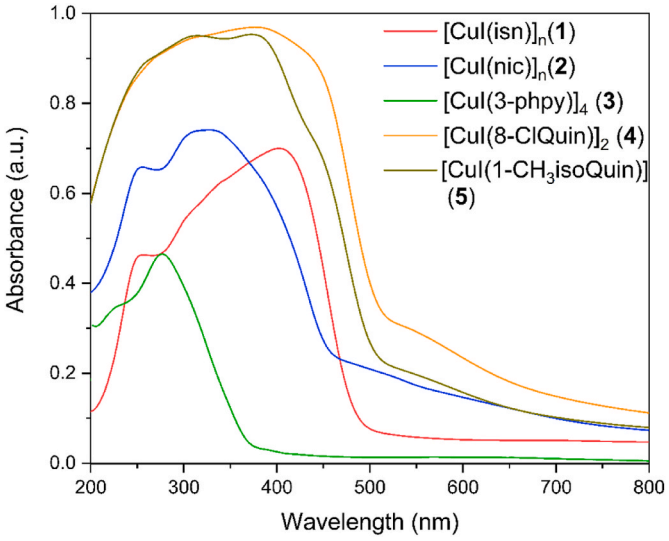

Fig. 9. Solid-state UV–Vis spectra of complexes **1**–**5** recorded at 298K from 200 to 800 nm.

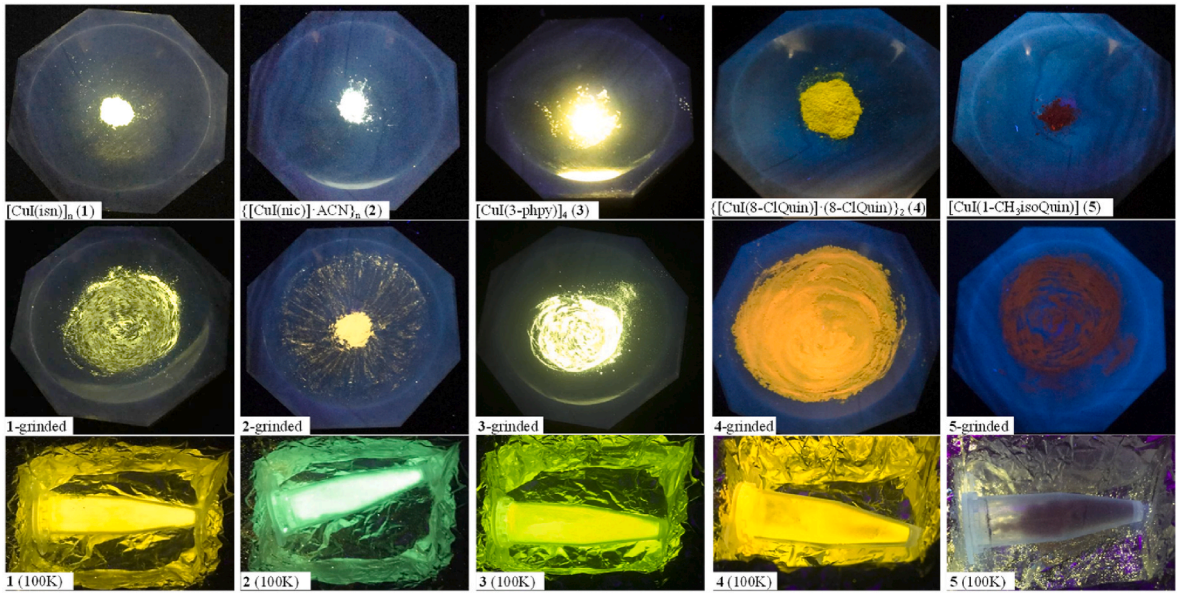

Fig. 8. Samples of **1**–**5** under 365 nm UV lamp exposure at 298K before (top), after (middle) grinding, or at 100K (bottom).

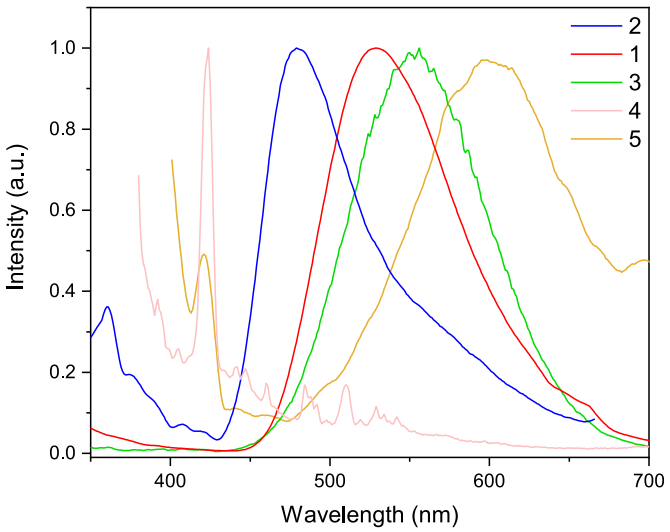

Fig. 10. Solid-state emission spectra of complexes **1**–**5** recorded at room temperature between 350 and 700 nm.

Table 9
Summary of the photophysical properties of complexes **1**–**5**. Reported data of absorption and emission maxima has been extracted from Ref. [66].

Sample	$\lambda_{abs\text{-}max}$ (nm)	$\lambda_{em\text{-}max}$ (nm)	Molecular arrangement	FWHM	Emission color	Stokes Shift (cm^{-1})
1	415	529	Staircase polymer	85.4	Yellow	5193
2	325	479	Staircase polymer	62.7	White	9892
3	275	552	Tetrameric Cubane	98.2	Yellow	18,248
4	380	413	Rhomboid Dimer	7.5	Blue	2103
5	375	600	Monomer	119.1	Orange	10,000
$[Cu_4I_4py_4]$	380	580	Tetrameric Cubane	–	Yellow	9074
$[CuIpy]_n$	362	437	Staircase polymer	–	Blue	4741
$[Cu_2I_2py_4]$	362	517	Rhomboid Dimer	–	Yellow	8282

ordered as py > nic > isn and the recorded emission wavelengths are ordered as py < nic < isn (Table 9).

One of the most demanded LEDs are white emitters, which are usually achieved by combination of blue LEDs (450–480 nm) usually coated with yellow (around 540 nm) single or multicomponent phosphors. Therefore, **1** and **3** could be used as coating phosphors for blue emitting LEDs whereas **2** directly provides white light since the inherent emission is the combination of two emission bands at 479 and 550 nm [5].

4. Calculations

Aiming to understand these properties, we performed DFT and TD-DFT calculations at the CAM-B3LYP level of theory with def2SVP basis sets for all elements (see computational details for further information). Due to the complexity of the materials; i.e. the registered UV–Vis spectra are obtained in the solid state with structures containing polymers, cubanes, dimers, or monomers highly interacting with the vicinal units; initial efforts were devoted to defining the computational model. Test calculations showed that complexes **1** and **2** should be represented with a polymer chain of at least four units interacting with the corresponding vicinal polymer chains. Indeed, the absence of vicinal chains leads to a helical structure resembling the structure of the ligands (S.I: Fig. S19) [68]. Moreover, in the case of **2**, the inclusion of the structural solvent molecules improved the results (S.I.: Fig. S20). On the other hand, for cubane, dimer, and monomer, the addition of 2, 4, and 4 vicinal units, respectively, is required to keep the structure of the central unit close to the solid state geometry, thus leading to a good representation of the absorption spectra. Remarkably, the use of smaller units in all cases leads to structures that are strongly different from those obtained with X-ray diffraction and, thus, they are not representative of the systems under study (S.I.: Figs. S19–S22).

The computed absorption spectra of the previously mentioned models of **1** to **5** were compared to the experimental ones providing a good fitting (Fig. 11). It is worth noting that the inclusion of several units of the discrete systems in the modeling is essential to reproduce the effect of transitions involving ligands of different units that appear at longer wavelengths. This is important especially due to the presence of aromatic rings that interact through π-stacking. Experimental absorption bands of polymer **1** at 403, 333, and 250 nm were computed to appear at 390, 322, and 264 nm, respectively. Likewise, absorption bands of the second polymer, **2**, at 450, 325, and 250 nm were shifted to 460, 330, and 270 nm in the calculated spectrum.

The discrete cubane, **3**, shows two absorption bands placed at 285 and 240 nm that are reproduced computationally by several intense bands around 280 nm. Finally, complexes **4** and **5** show a very broad absorption band that is also suggested by calculations. Thus, the difference between calculated and experimental absorption maxima differ by less than 30 nm, which is considered to be within the precision of the modeling approach [69].

Analysis of the molecular orbitals involved in the absorption process allows identifying the nature of the electronic transitions. Figs. 12 and 13 show the molecular orbitals involved in a representative electronic transition of **2** and **5**, respectively. The molecular orbitals involved in the representative transitions of the other complexes are reported in the S.I.: Figs. S23–S27. The main contributor to the absorption bands of all complexes originates from metal-halide to ligand charge transfer (M + X)LCT transitions. Indeed, the HOMOs are centered on the CuI moiety whereas LUMOs belong to the ligands. The unique exception is complex **3** (the cubane) which apart from the (M + X)LCT type of transitions also presents cluster-centered (^{3}CC) transitions. In particular, the absorption at energies between 315 and 280 nm belongs to (M + X)LCT transitions from Cu(I) and iodide to 3-phpy π orbitals. Instead, below ~280 nm, absorption presents a contribution from delocalized Cu(I) and iodide orbitals displaying an admixture of both transitions. This behavior agrees with the short Cu···Cu distance of 2.6141(4) Å in **3** which promotes strong contribution from ^{3}CC transitions.

Several previous computational studies were reported in the literature [66,70,71]. They mainly focus on discrete units of similar systems, while related polymers were only analyzed with the projected density of states (PDOS) of the crystal structure [6]. For dimers and monomers, it was suggested that the main contributors to the absorption spectra are (M + X)LCT transitions [72]. For polymers, the PDOS shows that the conduction band is composed of Cu(I) and iodide orbitals whereas the valence band has a major contribution from the ligands, thus suggesting again that the main transitions are composed of (M + X)LCT. Finally, there is a wide agreement that similar cubane systems show both cluster-centered and (M + X)LCT optical transitions. Therefore, the here presented systems show the same contributions to the optical spectra as related complexes already described in the literature.

5. Conclusions

Within this contribution, a series of five Cu(I)-iodide complexes were arranged by an easy one-pot synthesis and fully characterized. They demonstrated stability after grinding which eased their manipulation and avoided structural transformations. The incorporation of such structural directing factors as steric bulkiness and attractive forces

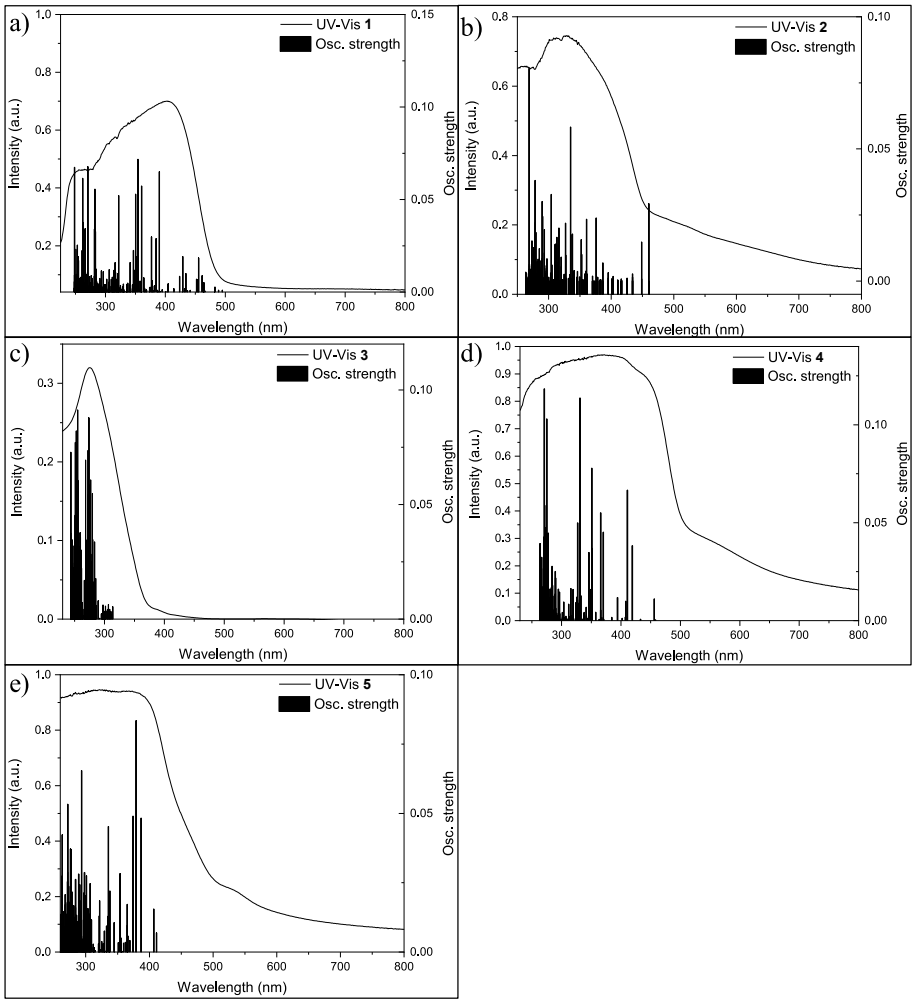

Fig. 11. Experimental UV–Vis spectra and calculated oscillator strength of complexes a) **1**; b) **2**; c) **3**; d) **4**; e) **5**.

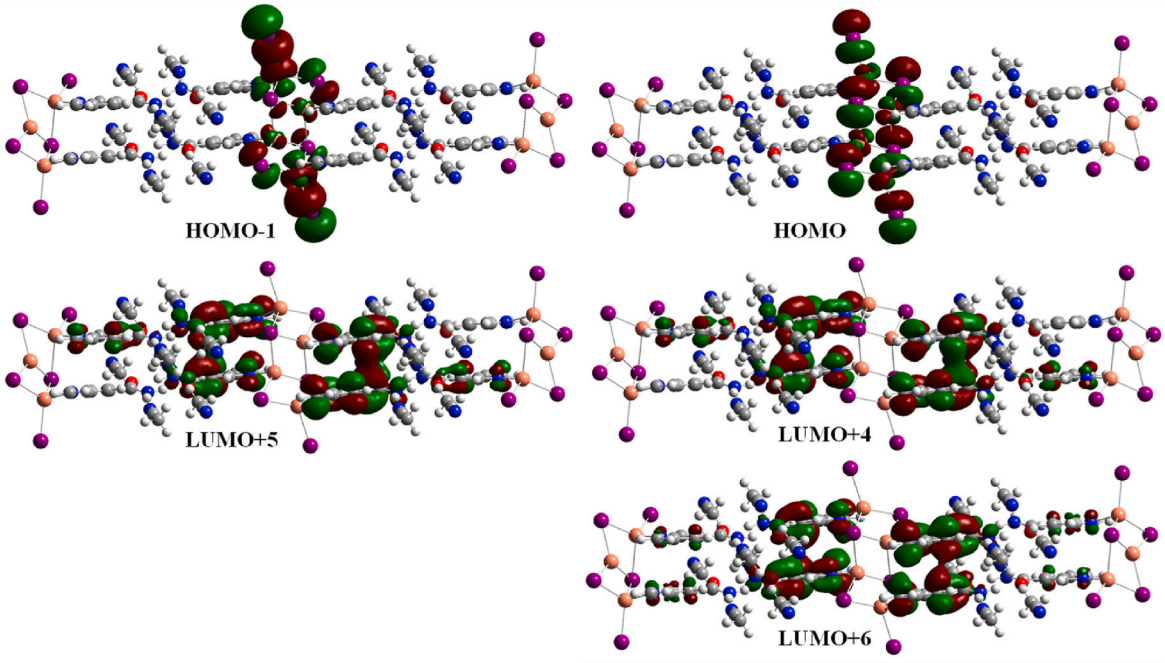

Fig. 12. Representation of the MOs of the electronic transition corresponding to TS 2 (λ = 460.07 nm) of complex **2**.

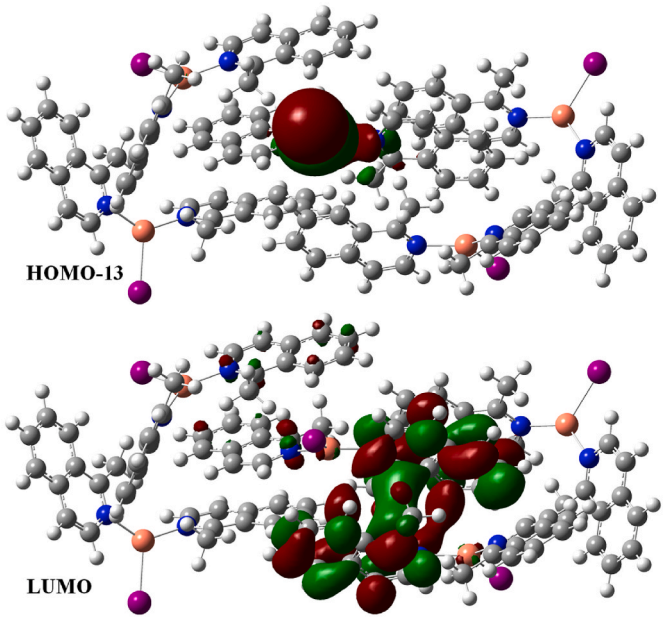

Fig. 13. Representation of the MOs of the electronic transition corresponding to TS 16 (λ = 353.80 nm) of complex **5**.

provided an additional degree of structural control. Then, *S* value distortion calculations evinced that cubane and staircase polymers are structurally closer than monomers and dimers, and suggested a pyramidalization or umbrella distortion pathway between both arrays. In addition, it was shown that cubanes accommodate greater distortions, thus facilitating structural transformations. Theoretical models support that the strong amide···amide interactions contribute to the ordering of the polymeric arrangement, and highlight the importance of π···π interactions within the structure of complexes **4** and **5**. Interestingly, modeling also revealed the importance of the occluded ACN molecule in **2** that strongly contributes to the structural arrangement and therefore, has an impact on the photophysical properties, emphasizing the influence of small changes to them. Therefore, complexes **1**–**5** exhibited emission properties dependent on the different arrangements and ligand functionalities, which displayed emission in the whole range of the visible spectrum. Thus, complexes **1**–**3** are potential candidates to be applied in the preparation of white LEDs as either direct or coated phosphors. We demonstrated the feasibility of calculating the absorption spectrum of Cu(I)-iodide staircase polymers that well reproduce the experimental spectrum. The TD-DFT calculations ensured that electronic transitions in the different arrangements originated from (M + X) LCT transitions and, therefore, absorption can be tuned either by modifying the arrangement which changes the HOMOs, or by the ligand, which provides the LUMOs.

CRediT authorship contribution statement

Francisco Sánchez-Férez: Writing – original draft, Visualization, Software, Methodology, Investigation, Formal analysis, Data curation, Conceptualization. **Xavier Solans-Monfort:** Writing – review & editing, Validation, Software, Resources, Project administration, Methodology, Funding acquisition, Data curation. **Luis Rodríguez-Santiago:** Writing – review & editing, Validation, Software, Resources, Project administration, Methodology, Funding acquisition, Data curation. **Teresa Calvet:** Writing – review & editing, Validation, Resources. **Mercè Font-Bardia:** Formal analysis, Data curation. **Josefina Pons:** Writing – review & editing, Validation, Supervision, Resources, Project administration, Funding acquisition, Conceptualization.

Declaration of competing interest

The authors declare that they have no known competing financial interests or personal relationships that could have appeared to influence the work reported in this paper.

Data availability

Data will be made available on request.

Acknowledgements

J.P. acknowledges financial support from the CB615921 project, the CB616406 project from "Fundació La Caixa" and the 2017SGR1687 project from the Generalitat de Catalunya. X.S.-M. and L.R.-S acknowledges financial support from MICINN (PID2020-112715 GB-I00). F.S.-F. acknowledges the PIF pre-doctoral fellowship from the Universitat Autònoma de Barcelona.

Appendix A. Supplementary data

Supplementary data to this article can be found online at https://doi.org/10.1016/j.jssc.2024.124639.

References

[1] S.R. Chemler, Copper catalysis in organic synthesis, Beilstein J. Org. Chem. 11 (2015) 2252–2253, https://doi.org/10.3762/bjoc.11.244.
[2] Y. Pan, R. Abazari, B. Tahir, S. Sanati, Y. Zheng, M. Tahir, J. Gao, Iron-based metal–organic frameworks and their derived materials for photocatalytic and photoelectrocatalytic reactions, Coord. Chem. Rev. 499 (2024) 215538, https://doi.org/10.1016/j.ccr.2023.215538.
[3] Z. Liu, J. Qiu, F. Wei, J. Wang, X. Liu, M.G. Helander, S. Rodney, Z. Wang, Z. Bian, Z. Lu, M.E. Thompson, C. Huang, Simple and high efficiency phosphorescence organic light-emitting diodes with codeposited copper(I) emitter, Chem. Mater. 26 (2014) 2368–2373, https://doi.org/10.1021/cm5006086.
[4] D. Volz, M. Wallesch, S.L. Grage, J. Göttlicher, R. Steininger, D. Batchelor, T. Vitova, A.S. Ulrich, C. Heske, L. Weinhardt, T. Baumann, S. Bräse, Labile or stable: can homoleptic and heteroleptic PyrPHOS–copper complexes Be processed from solution? Inorg. Chem. 53 (2014) 7837–7847, https://doi.org/10.1021/ic500135m.
[5] W. Liu, Y. Fang, J. Li, Copper iodide based hybrid phosphors for energy-efficient general lighting technologies, Adv. Funct. Mater. 28 (2018) 1705593, https://doi.org/10.1002/adfm.201705593.
[6] S. Wang, E.E. Morgan, S. Panuganti, L. Mao, P. Vishnoi, G. Wu, Q. Liu, M. G. Kanatzidis, R.D. Schaller, R. Seshadri, Ligand control of structural diversity in luminescent hybrid copper(I) iodides, Chem. Mater. 34 (2022) 3206–3216, https://doi.org/10.1021/acs.chemmater.1c04408.
[7] P. Healy, J. Kildea, B. Skelton, A. White, Lewis-Base adducts of group 11 metal(I) compounds. XLIII. Synthesis and structural systematics of 1 : 1 copper(I) halide/nitrogen base adducts as $[(N\text{-base})_1(CuX)_1]_\infty$ "split-stair" polymers (X = Cl, Br, I; N-base = acridine, quinaldine, Aust. J. Chem. 42 (1989) 115, https://doi.org/10.1071/CH9890115.
[8] F. Farinella, L. Maini, P.P. Mazzeo, V. Fattori, F. Monti, D. Braga, White luminescence achieved by a multiple thermochromic emission in a hybrid organic–inorganic compound based on 3-picolylamine and copper(I) iodide, Dalton Trans. 45 (2016) 17939–17947, https://doi.org/10.1039/C6DT03049A.
[9] L. Maini, D. Braga, P.P. Mazzeo, B. Ventura, Polymorph and isomer conversion of complexes based on CuI and PPh_3 easily observed via luminescence, Dalton Trans. 41 (2012) 531–539, https://doi.org/10.1039/C1DT11462J.
[10] S. Cho, Y. Jeon, S. Lee, J. Kim, T.H. Kim, Reversible transformation between cubane and stairstep Cu_4I_4 clusters using heat or solvent vapor, Chem. Eur J. 21 (2015) 1439–1443, https://doi.org/10.1002/chem.201405800.
[11] T.H. Kim, Y.W. Shin, J.H. Jung, J.S. Kim, J. Kim, Crystal-to-Crystal transformation between three Cu^I coordination polymers and structural evidence for luminescence thermochromism, Angew. Chem. Int. Ed. 47 (2008) 685–688, https://doi.org/10.1002/anie.200704349.
[12] S. Naik, J.T. Mague, M.S. Balakrishna, Short-bite PNP ligand-supported rare tetranuclear $[Cu_4I_4]$ clusters: structural and photoluminescence studies, Inorg. Chem. 53 (2014) 3864–3873, https://doi.org/10.1021/ic500240j.
[13] B. Huitorel, H. El Moll, M. Cordier, A. Fargues, A. Garcia, F. Massuyeau, C. Martineau-Corcos, T. Gacoin, S. Perruchas, Luminescence mechanochromism induced by cluster isomerization, Inorg. Chem. 56 (2017) 12379–12388, https://doi.org/10.1021/acs.inorgchem.7b01870.
[14] Q. Benito, X.F. Le Goff, G. Nocton, A. Fargues, A. Garcia, A. Berhault, S. Kahlal, J.-Y. Saillard, C. Martineau, J. Trébosc, T. Gacoin, J.-P. Boilot, S. Perruchas, Geometry flexibility of copper iodide clusters: variability in luminescence

thermochromism, Inorg. Chem. 54 (2015) 4483–4494, https://doi.org/10.1021/acs.inorgchem.5b00321.
[15] J. Conesa-Egea, F. Zamora, P. Amo-Ochoa, Perspectives of the smart Cu-Iodine coordination polymers: a portage to the world of new nanomaterials and composites, Coord. Chem. Rev. 381 (2019) 65–78, https://doi.org/10.1016/j.ccr.2018.11.008.
[16] A. Aguirrechu-Comerón, R. Hernández-Molina, P. Rodríguez-Hernández, A. Muñoz, U.R. Rodríguez-Mendoza, V. Lavín, R.J. Angel, J. Gonzalez-Platas, Experimental and ab initio study of catena(bis(μ_2-iodo)-6-methylquinoline-copper (I)) under pressure: synthesis, crystal structure, electronic, and luminescence properties, Inorg. Chem. 55 (2016) 7476–7484, https://doi.org/10.1021/acs.inorgchem.6b00796.
[17] J. Soldevila-Sanmartín, E. Ruiz, D. Choquesillo-Lazarte, M.E. Light, C. Viñas, F. Teixidor, R. Núñez, J. Pons, J.G. Planas, Tuning the architectures and luminescence properties of Cu(I) compounds of phenyl and carboranyl pyrazoles: the impact of 2D versus 3D aromatic moieties in the ligand backbone, J. Mater. Chem. C 9 (2021) 7643–7657, https://doi.org/10.1039/d1tc01395e.
[18] S. Nagaoka, Y. Ozawa, K. Toriumi, M. Abe, A dual-emission strategy for a wide-range phosphorescent color-tuning of a crystalline-state molecular cluster [Cu_4I_4(2-bzpy)$_4$] (2-bzpy = 2-benzylpyridine), Chem. Lett. 47 (2018) 1101–1104, https://doi.org/10.1246/cl.180435.
[19] S. Perruchas, Molecular copper iodide clusters: a distinguishing family of mechanochromic luminescent compounds, Dalton Trans. 50 (2021) 12031–12044, https://doi.org/10.1039/D1DT01827B.
[20] L. Maini, D. Braga, P.P. Mazzeo, L. Maschio, M. Rérat, I. Manet, B. Ventura, Dual luminescence in solid CuI(piperazine): hypothesis of an emissive 1-D delocalized excited state, Dalton Trans. 44 (2015) 13003–13006, https://doi.org/10.1039/C5DT02204E.
[21] K. Tsuge, Y. Chishina, H. Hashiguchi, Y. Sasaki, M. Kato, S. Ishizaka, N. Kitamura, Luminescent copper(I) complexes with halogenido-bridged dimeric core, Coord. Chem. Rev. 306 (2016) 636–651, https://doi.org/10.1016/j.ccr.2015.03.022.
[22] T. Sengupta, T.T. Dang, J.S. Chung, S.G. Kang, Insight into the structure and bonding of copper(I) iodide clusters and a cluster-based coordination polymer, New J. Chem. 43 (2019) 16176–16187, https://doi.org/10.1039/C9NJ02130B.
[23] F. Sánchez-Férez, J.M. Rius-Bartra, J.A. Ayllón, T. Calvet, M. Font-Bardia, J. Pons, Tuning photophysical properties by p-functional groups in Zn(II) and Cd(II) complexes with piperonylic acid, Molecules 27 (2022) 1365, https://doi.org/10.3390/molecules27041365.
[24] F. Sánchez-Férez, X. Solans-Monfort, T. Calvet, M. Font-Bardia, J. Pons, Controlling the formation of two concomitant polymorphs in Hg(II) coordination polymers, Inorg. Chem. 61 (2022), https://doi.org/10.1021/acs.inorgchem.1c03762, 4965–497.
[25] L. Leiserowitz, G.M.J. Schmidt, Molecular packing modes. Part III. Primary amides, J. Chem. Soc. A Inorganic, Phys. Theor. (1969) 2372–2382, https://doi.org/10.1039/j19690002372.
[26] G.M. Sheldrick, A short history of SHELX, Acta Crystallogr. A. 64 (2008) 112–122, https://doi.org/10.1107/S0108767307043930.
[27] M. Llunell, D. Casanova, J. Cirera, P. Alemany, S. Alvarez, SHAPE. Program for the Stereochemical Analysis of Molecular Fragments by Means of Continuous Shape Measures and Associated Tools, Universitat de Barcelona, Barcelona (2013).
[28] M. Pinsky, D. Avnir, Continuous symmetry measures. 5. The classical polyhedra, Inorg. Chem. 37 (1998) 5575–5582, https://doi.org/10.1021/ic9804925.
[29] C.F. MacRae, I. Sovago, S.J. Cottrell, P.T.A. Galek, P. McCabe, E. Pidcock, M. Platings, G.P. Shields, J.S. Stevens, M. Towler, P.A. Wood, Mercury 4.0: from visualization to analysis, design and prediction, J. Appl. Crystallogr. 53 (2020) 226–235, https://doi.org/10.1107/S1600576719014092.
[30] Persistence of Vision Pt. Ltd. Persistence of Vision (TM) Raytracer, Williamstown, Australia, 2004 [Computer software] Version 3.6.
[31] M.J. Frisch, G.W. Trucks, H.B. Schlegel, G.E. Scuseria, M.A. Robb, J.R. Cheeseman, G. Scalmani, V. Barone, G.A. Petersson, H. Nakatsuji, X. Li, M. Caricato, A. V Marenich, J. Bloino, B.G. Janesko, R. Gomperts, B. Mennucci, H.P. Hratchian, J. V Ortiz, A.F. Izmaylov, J.L. Sonnenberg, D. Williams-Young, F. Ding, F. Lipparini, F. Egidi, J. Goings, B. Peng, A. Petrone, T. Henderson, D. Ranasinghe, V. G. Zakrzewski, J. Gao, N. Rega, G. Zheng, W. Liang, M. Hada, M. Ehara, K. Toyota, R. Fukuda, J. Hasegawa, M. Ishida, T. Nakajima, Y. Honda, O. Kitao, H. Nakai, T. Vreven, K. Throssell, J.A. Montgomery Jr., J.E. Peralta, F. Ogliaro, M. J. Bearpark, J.J. Heyd, E.N. Brothers, K.N. Kudin, V.N. Staroverov, T.A. Keith, R. Kobayashi, J. Normand, K. Raghavachari, A.P. Rendell, J.C. Burant, S.S. Iyengar, J. Tomasi, M. Cossi, J.M. Millam, M. Klene, C. Adamo, R. Cammi, J.W. Ochterski, R.L. Martin, K. Morokuma, O. Farkas, J.B. Foresman, D.J. Fox, Gaussian 16 Revision C.01, 2016.
[32] T. Yanai, D.P. Tew, N.C. Handy, A new hybrid exchange–correlation functional using the Coulomb-attenuating method (CAM-B3LYP), Chem. Phys. Lett. 393 (2004) 51–57, https://doi.org/10.1016/j.cplett.2004.06.011.
[33] J. Moellmann, S. Grimme, DFT-D3 study of some molecular crystals, J. Phys. Chem. C 118 (2014) 7615–7621, https://doi.org/10.1021/jp501237c.
[34] F. Weigend, R. Ahlrichs, Balanced basis sets of split valence, triple zeta valence and quadruple zeta valence quality for H to Rn: design and assessment of accuracy, Phys. Chem. Chem. Phys. 7 (2005) 3297, https://doi.org/10.1039/b508541a.
[35] F. Weigend, Accurate Coulomb-fitting basis sets for H to Rn, Phys. Chem. Chem. Phys. 8 (2006) 1057, https://doi.org/10.1039/b515623h.
[36] P.J. Stephens, F.J. Devlin, C.F. Chabalowski, M.J. Frisch Ab, Initio Calculation of Vibrational Absorption and Circular Dichroism Spectra Using Density Functional Force Fields, J. Phys. Chem. 98 (1994) 11623–11627. https://doi.org/10.1021/j100096a001.
[37] M.J. Frisch, J.A. Pople, J.S. Binkley, Self-consistent molecular orbital methods 25. Supplementary functions for Gaussian basis sets, J. Chem. Phys. 80 (1984) 3265–3269, https://doi.org/10.1063/1.447079.
[38] Y. Ji, X. Yang, Z. Ji, L. Zhu, N. Ma, D. Chen, X. Jia, J. Tang, Y. Cao, DFT-calculated IR spectrum amide I, II, and III band contributions of N -methylacetamide fine components, ACS Omega 5 (2020) 8572–8578, https://doi.org/10.1021/acsomega.9b04421.
[39] X.-M. Li, J. Jia, D. Yang, J. Jin, J. Gao, Construction of biomimetic proton transport channels in metal-organic framework, Chin. Chem. Lett. 35 (2024) 108474, https://doi.org/10.1016/j.cclet.2023.108474.
[40] Y.A. Kwon, C. Lee, S. Park, Effect of ion-molecule interaction on fermi-resonance in acetonitrile studied by ultrafast vibrational spectroscopy, Chem. Phys. 445 (2014) 38–45, https://doi.org/10.1016/j.chemphys.2014.10.017.
[41] S. Scheiner, Ability of IR and NMR spectral data to distinguish between a tetrel bond and a hydrogen bond, J. Phys. Chem. A 122 (2018) 7852–7862, https://doi.org/10.1021/acs.jpca.8b07631.
[42] M. Sevukarajan, B. Thanuja, R. Sodanapalli, R. Nair, Synthesis and characterization of a pharmaceutical co-crystal:(Aceclofenac:Nicotinamide), J. Pharmaceut. Sci. Res. 3 (2011) 1288–1293.
[43] K. Nakamoto, Infrared and Raman Spectra of Inorganic and Coordination Compounds Part A: Theory and Applications, sixth ed., Wiley, Hoboken, New Jersey, USA, 2009.
[44] I. Fleming, D. Williams, Spectroscopic Methods in Organic Chemistry, seventh ed., Springer International Publishing, Cham, 2008 https://doi.org/10.1007/978-3-030-18252-6.
[45] G.M. Leskowitz, N. Ghaderi, R.A. Olsen, K. Pederson, M.E. Hatcher, L.J. Mueller, The amide rotational barrier in isonicotinamide: dynamic NMR and Ab initio studies, J. Phys. Chem. A 109 (2005) 1152–1158, https://doi.org/10.1021/jp0460689.
[46] S. Wang, E.E. Morgan, S. Panuganti, L. Mao, P. Vishnoi, G. Wu, Q. Liu, M. G. Kanatzidis, R.D. Schaller, R. Seshadri, Ligand control of structural diversity in luminescent hybrid copper(I) iodides, Chem. Mater. 34 (2022) 3206–3216, https://doi.org/10.1021/acs.chemmater.1c04408.
[47] P. Healy, J. Kildea, B. Skelton, A. White, Lewis-Base adducts of group 11 metal(I) compounds. XLI. Conformational systematics of [(N-base)$_1$(CuX)$_1$]$_\infty$ "skewed stair" polymers [N-base = (substituted) pyridine], Aust. J. Chem. 42 (1989) 93, https://doi.org/10.1071/CH9890093.
[48] S. Saha, G.R. Desiraju, Acid···Amide supramolecular synthon in cocrystals: from spectroscopic detection to property engineering, J. Am. Chem. Soc. 140 (2018) 6361–6373, https://doi.org/10.1021/jacs.8b02435.
[49] P.R. Varadwaj, A. Varadwaj, H.M. Marques, K. Yamashita, Definition of the tetrel bond, CrystEngComm 25 (2023) 1411–1423, https://doi.org/10.1039/D2CE01621D.
[50] N.V.S. Harisomayajula, S. Makovetskyi, Y.C. Tsai, Cuprophilic interactions in and between molecular entities, Chem. Eur J. 25 (2019) 8936–8954, https://doi.org/10.1002/chem.201900332.
[51] M.R. Churchill, G. Davies, M.A. El-Sayed, J.P. Hutchinson, M.W. Rupich, Synthesis, structure, and properties of the tetranuclear complexes [(DENC)CuX]$_4$ (DENC = N, N-diethylnicotinamide; X = Cl, Br, I) and the kinetics of oxidation of the chloride and bromide by dioxygen in aprotic solvents, Inorg. Chem. 21 (1982) 995–1001, https://doi.org/10.1021/ic00133a025.
[52] W.J. Gee, S.R. Batten, Cuprous halide complexes of a variable length ligand: helices, cluster chains, and nets containing large solvated channels, Cryst. Growth Des. 13 (2013) 2335–2343, https://doi.org/10.1021/cg3018858.
[53] S. Hu, M.L. Tong, Rational design and construction of the first tetrahedral net with photoluminescent Cu_4I_4 cubane cluster as the tetrahedral nodet, Dalton Trans. (2005) 1165–1167, https://doi.org/10.1039/b500015g.
[54] C.R. Groom, I.J. Bruno, M.P. Lightfoot, S.C. Ward, The Cambridge structural database, Acta Crystallogr. Sect. B Struct. Sci. Cryst. Eng. Mater. 72 (2016) 171–179, https://doi.org/10.1107/S2052520616003954.
[55] S. Keinan, D. Avnir, Continuous symmetry analysis of tetrahedral/planar distortions. Copper chlorides and other AB_4 species, Inorg. Chem. 40 (2001) 318–323, https://doi.org/10.1021/ic000681z.
[56] O.Y. Khyzhun, V.L. Bekenev, O.V. Parasyuk, S.P. Danylchuk, N.M. Denysyuk, A. O. Fedorchuk, N. AlZayed, I.V. Kityk, Single crystal growth and the electronic structure of orthorhombic Tl_3PbBr_5: a novel material for non-linear optics, Opt. Mater. 35 (2013) 1081–1089, https://doi.org/10.1016/j.optmat.2012.12.008.
[57] O.Y. Khyzhun, V.L. Bekenev, N.M. Denysyuk, I.V. Kityk, P. Rakus, A.O. Fedorchuk, S.P. Danylchuk, O.V. Parasyuk, Single crystal growth and the electronic structure of TlPb2Br5, Opt. Mater. 36 (2013) 251–258, https://doi.org/10.1016/j.optmat.2013.09.004.
[58] O.Y. Khyzhun, V.L. Bekenev, N.M. Denysyuk, O.V. Parasyuk, A.O. Fedorchuk, First-principles band-structure calculations and X-ray photoelectron spectroscopy studies of the electronic structure of $TlPb_2Cl_5$, J. Alloys Compd. 582 (2014) 802–809, https://doi.org/10.1016/j.jallcom.2013.08.127.
[59] J. Cirera, P. Alemany, S. Alvarez, Mapping the stereochemistry and symmetry of tetracoordinate transition-metal complexes, Chem. Eur J. 10 (2004) 190–207, https://doi.org/10.1002/chem.200305074.
[60] S. Alvarez, Distortion pathways of transition metal coordination polyhedra induced by chelating topology, Chem. Rev. 115 (2015) 13447–13483, https://doi.org/10.1021/acs.chemrev.5b00537.
[61] J. Vela, J. Cirera, J.M. Smith, R.J. Lachicotte, C.J. Flaschenriem, S. Alvarez, P. L. Holland, Quantitative geometric descriptions of the belt iron atoms of the Iron−Molybdenum cofactor of nitrogenase and synthetic iron(II) model complexes, Inorg. Chem. 46 (2007) 60–71, https://doi.org/10.1021/ic0609148.

[62] E. Cariati, X. Bu, P.C. Ford, Solvent- and vapor-induced isomerization between the luminescent solids $[CuI(4\text{-pic})]_4$ and $[CuI(4\text{-pic})]_\infty$ (pic = methylpyridine). The structural basis for the observed luminescence vapochromism, Chem. Mater. 12 (2000) 3385–3391, https://doi.org/10.1021/cm0010708.

[63] Q. Benito, I. Maurin, M. Poggi, C. Martineau-Corcos, T. Gacoin, J.-P. Boilot, S. Perruchas, Impact of crystalline packing on the mechanochromic luminescence properties of copper based compounds: towards functional coatings, J. Mater. Chem. C 4 (2016) 11231–11237, https://doi.org/10.1039/C6TC04262G.

[64] Y. Lv, J. Yang, H. Li, W. Liu, G. Ouyang, Molecular design towards efficient light-emitting copper(I) halide mononuclear hybrids, Mater. Adv. 5 (2024) 1234–1239, https://doi.org/10.1039/D3MA00904A.

[65] A. Mensah, J.J. Shao, J.L. Ni, G.J. Li, F.M. Wang, L.Z. Chen, Recent progress in luminescent Cu(I) halide complexes: a mini-review, Front. Chem. 9 (2022) 1–7, https://doi.org/10.3389/fchem.2021.816363.

[66] K.R. Kyle, C.K. Ryu, P.C. Ford, J.A. DiBenedetto, Photophysical studies in solution of the tetranuclear copper(I) clusters $Cu_4I_4L_4$ (L = pyridine or substituted pyridine), J. Am. Chem. Soc. 113 (1991) 2954–2965, https://doi.org/10.1021/ja00008a026.

[67] E.S.H. El Ashry, A. El Nemr, S. Ragab, Quantitative structure activity relationships of some pyridine derivatives as corrosion inhibitors of steel in acidic medium, J. Mol. Model. 18 (2012) 1173–1188, https://doi.org/10.1007/s00894-011-1148-7.

[68] N. Fellah, C.J. Zhang, C. Chen, C.T. Hu, B. Kahr, M.D. Ward, A.G. Shtukenberg, Highly polymorphous nicotinamide and isonicotinamide: solution versus melt crystallization, Cryst. Growth Des. 21 (2021) 4713–4724, https://doi.org/10.1021/acs.cgd.1c00547.

[69] C. Adamo, D. Jacquemin, The calculations of excited-state properties with time-dependent density functional theory, Chem. Soc. Rev. 42 (2013) 845–856, https://doi.org/10.1039/C2CS35394F.

[70] M. Vitale, W.E. Palke, P.C. Ford, Origins of the double emission of the tetranuclear copper(I) cluster $Cu_4I_4(pyridine)_4$: an ab initio study, J. Phys. Chem. 96 (1992) 8329–8336, https://doi.org/10.1021/j100200a023.

[71] S. Gholipour, A.M. Ali, J.-P. Correa-Baena, S.-H. Turren-Cruz, F. Tajabadi, W. Tress, N. Taghavinia, M. Grätzel, A. Abate, F. De Angelis, C.A. Gaggioli, E. Mosconi, A. Hagfeldt, M. Saliba, Globularity-selected large molecules for a new generation of multication perovskites, Adv. Mater. 29 (2017) 1702005, https://doi.org/10.1002/adma.201702005.

[72] L. Yang, J. Feng, A. Ren, M. Zhang, Y. Ma, X. Liu, Structures, electronic states and electroluminescent properties of a series of Cu^I complexes, Eur. J. Inorg. Chem. (2005) 1867, https://doi.org/10.1002/ejic.200400941. –1879.